energies

MDPI

Article

Operational Simulation and Performance Evaluation of Electricity Energy Markets Using WoLF-PHC Multi-Agent Reinforcement Learning

Zhengpai Cui [1], Xiaoxue Liu [1], Xue Gong [1], Yu Gong [2,*], Yang Zhao [2] and Yinchi Shao [2]

[1] State Grid Jibei Electric Power Company Limited, Beijing 100052, China; cui.zhengpai@jibei.sgcc.com.cn (Z.C.); snowwhite_liu@126.com (X.L.); shufegx@foxmail.com (X.G.)
[2] State Grid Jibei Electric Power Co., Ltd., Electric Power Science Research Institute, Beijing 100045, China; zhao.yang@jibei.sgcc.com.cn (Y.Z.); shao.yinchi@jibei.sgcc.com.cn (Y.S.)
* Correspondence: gongyusg@126.com

Abstract

As the share of wind and photovoltaic generation in power systems increases, renewable generation and storage are increasingly participating in bidding in electricity markets. However, fluctuations in renewable output, uncertain market prices, and intertemporal coupling in storage operation complicate bidding and increase operating risks. This study develops an electricity energy market simulation framework covering medium- and long-term trading and spot-market trading. The Win or Learn Fast policy hill-climbing (WoLF-PHC) algorithm is used to model multi-agent bidding, accounting for contract settlement, deviation assessment, operating characteristics of conventional units, and constraints on the storage state of charge. Joint renewable-storage operation and independent participation are compared in terms of policy convergence, participant operating profit, consumer procurement cost, renewable utilization, and storage operation. The case study supports the effectiveness of the framework and shows that market participants can develop stable bidding policies. Compared with independent participation, joint operation coordinates energy internally between renewable plants and storage facilities, improving system operating performance while reducing consumer procurement costs and promoting renewable utilization.

Keywords: electricity energy market; renewable energy; energy storage; multi-agent reinforcement learning; WoLF-PHC; bidding strategy

1. Introduction

Global decarbonization and the development of modern power systems continue to drive growth in installed wind and photovoltaic (PV) capacity. The generation mix is shifting from controllable fossil-fuel resources toward coordinated operation of diverse energy resources [1,2]. Meanwhile, electricity-market reform in China has expanded trading from medium- and long-term contracts to spot and ancillary-service markets, strengthening the role of price signals in resource allocation. Renewable producers have consequently evolved from passive recipients of guaranteed purchases into market participants that compete and bear responsibility for deviations. Energy storage has also become integral to market operation and value formation because it can shift energy over time and respond rapidly [3,4]. Effective coordination between contracts and real-time markets is therefore essential for balancing short-term operating efficiency, risk management, and long-term investment incentives [5].

Check for updates

Academic Editor: Jianjian Shen

Received: 21 September 2026
Revised: 7 November 2026
Accepted: 11 November 2026
Published: 20 November 2026

Copyright: © 2026 by the authors. Licensee MDPI, Basel, Switzerland. This article is an open access article distributed under the terms and conditions of the Creative Commons Attribution (CC BY) license.

Renewable output is stochastic and variable, and forecast errors create differences between scheduled and actual generation. These differences can trigger imbalance settlement, deviation penalties, and revenue losses. Supply–demand conditions, strategic behavior, and policy changes further amplify price uncertainty [6,7]. As variable generation increases, systems require more balancing of resources and operating flexibility, making balancing markets increasingly important [8]. Resource endowments, weather, and electricity prices also cause revenue risk for renewable producers to span multiple time scales [9]. Storage can mitigate renewable deviations through charging and discharging. However, its operation is constrained by power ratings, state of charge (SOC), conversion efficiency, cycle life, and intertemporal energy balance. Changing market conditions also require a trade-off between flexibility and operating cost [10]. Coordinating forecast errors, price risk, physical constraints, and strategic behavior under incomplete information is central to participant profitability and system efficiency [11].

Existing bidding methods address these challenges through mathematical optimization, game-theoretic analysis, price forecasting, and intelligent decision-making. Stochastic programming represents output and price uncertainty through scenarios; robust optimization controls adverse-scenario risk through uncertainty sets; and bilevel programming captures the nested relationship between participant bids and market clearing [12–14]. Although mathematically explicit, these methods commonly require assumed probability distributions, complete information, or an exact market model, and may suffer from scenario proliferation and non-convexity. Traditional electricity-market studies have also examined market power and its influence on strategic bidding [15]. Cooperative, non-cooperative, Stackelberg, and evolutionary games provide systematic tools for representing strategic interactions among participants [13,14,16]. Price forecasts supply external information for bidding and have progressed from statistical and machine-learning models to deep learning, with increasing emphasis on common datasets, benchmarks, and evaluation protocols [17–20]. Forecast accuracy, however, does not necessarily yield optimal bids. Single-agent reinforcement learning updates policies directly from environmental feedback but generally treats other participants as part of the environment, inadequately representing the non-stationarity created when multiple learning agents act simultaneously [21,22].

Electricity markets inherently involve participants with different objectives, information, and constraints, making multi-agent methods well suited to their distributed decision structure. Early studies modeled generating units, distributed resources, storage, and consumers as interacting autonomous agents and used distributed algorithms for task allocation, information exchange, and market coordination [23]. Agent-based market simulations further showed that learning rules and risk preferences alter competition and market outcomes, so bidding models must explicitly represent interactions among participants [24]. Multi-agent reinforcement learning formalizes states, actions, rewards, and inter-agent coupling within a Markov game, enabling participants to update their policies from local observations, clearing outcomes, and profit feedback. Centralized training with decentralized execution can use joint information during training to improve stability while relying only on locally available information during actual decisions. This provides a general framework for partial observability, credit assignment, growth in the joint action space, and equilibrium selection [25].

Multi-agent research on strategic generator bidding initially focused on competitive equilibria and policy learning in day-ahead markets. Du et al. (2021) modeled generators as learning agents and used multi-agent deterministic policy gradients to approximate day-ahead Nash equilibrium under partial observability [26]. Their results supported the feasibility of interactive learning for strategic bidding. Subsequent work developed participant-specific bidding frameworks whose state spaces include historical clearing

information, market conditions, and rival behavior, thereby producing more adaptive bid policies [27]. To address market-rule changes and limited training samples, Wu et al. (2022) transferred policy knowledge from a source market to a target market [28]. This approach shortened training and improved decisions under new rules. Collectively, these studies show that multi-agent methods can incorporate competitors' evolving strategies into continual learning rather than treating other participants as a fixed environment.

As renewable and storage participation has deepened, multi-agent bidding research has expanded beyond competition among homogeneous generators. It now covers coordinated operation across renewable resources, storage systems, and multiple markets. Studies of storage participation in energy and frequency-regulation markets model wind power, conventional generation, and storage as distinct agents. Their joint state space represents charging and discharging power, regulation capacity, and intertemporal state of charge, thereby capturing how storage allocates flexibility among services [10]. Multi-agent models for joint wind-thermal-storage bidding account for renewable deviations, conventional-unit costs, and rapid storage response. These models coordinate competition across energy and regulation markets [29]. Two-stage models also combine day-ahead price forecasts informed by carbon, green-certificate, and fuel prices with multi-agent bidding decisions. This approach links the behavior of wind, hydropower, thermal generation, and purchasers directly to market objectives [30].

Unlike metaheuristic global optimization algorithms, such as the Musical Chairs Algorithm (MCA) and the Star-Nosed Mole Optimizer (SNMO) [31,32], multi-agent methods such as the Win or Learn Fast policy hill-climbing (WoLF-PHC) algorithm do not directly solve optimization problems for storage sizing. Instead, they evaluate the market returns of renewable plants at a given storage capacity by analyzing bidding decisions and profits. In retail markets, multi-agent reinforcement learning can combine consumers' price perceptions with demand response to represent bilateral bidding between retailers and consumers [33]. Evolutionary games combined with Q-learning and swarm intelligence can describe limited information and strategy evolution in end-user demand-response bids [34]. In coupled electricity, carbon, and green-certificate markets, agents can adapt their transactions simultaneously, revealing how price linkages and policy mechanisms affect profits and energy choices [35]. Continuous double-auction studies place agents on both the supply and demand sides to simulate bilateral bidding and network-constrained clearing [36]. For decentralized renewable-energy trading, evolutionary-game studies further reveal dynamic strategy adjustment as the competitive environment changes [37].

Overall, multi-agent algorithms can represent bidding competition among renewable generators, storage systems, thermal generators, hydropower generators, and consumers in a common market. They update bids iteratively from repeated clearing outcomes. Each generator selects a piecewise bid curve, and market clearing determines its awarded quantity and the market-clearing price (MCP). The generator then calculates its return from revenue from electricity sales, generation cost, contract settlement, and deviation charges. Higher-return bids consequently become more likely to be selected again. Two gaps remain in simulation-based analyses of electricity energy market bidding decisions. The first concerns a closed-loop framework linking bidding, clearing, operation, and settlement, including medium- and long-term contract settlement through contracts for difference (CfDs), K-recovery, and deviation assessment. The second concerns the analysis of bidding strategies and returns within a unified electricity energy market simulation framework.

To address these gaps, this study develops an electricity energy market simulation framework covering medium- and long-term and spot markets. It investigates strategic bidding and operational performance when renewable generation and storage participate across multiple market time scales. The main contributions are as follows:

(1) This study develops a coordinated electricity energy market simulation framework linking medium- and long-term trading with spot-market operation. Monthly and weekly trading are integrated with day-ahead, intraday, and real-time stages. Decomposition of contract energy, CfD settlement, real-time deviation assessment, and the periodic K-recovery mechanism link contract performance across these markets. Thermal-unit start-up, shutdown, and ramping limits, uncertainty in renewable output, and storage state-of-charge constraints are incorporated into a closed loop of bidding, clearing, operation, and settlement. A heterogeneous WoLF-PHC multi-agent bidding model represents thermal-power, hydropower, wind-storage, photovoltaic-storage, and demand-side participants as independent agents. Action spaces are defined for non-decreasing piecewise bids and load adjustments, and rewards combine spot-market returns, CfD settlement, K-recovery, deviation smoothing, and storage value. WoLF-PHC adjusts policies slowly when winning and quickly when losing, allowing participants to adapt their bids competitively and linking market simulation with bidding decisions.

(2) This study establishes a multidimensional evaluation framework covering algorithmic, electricity energy market, and physical operating performance. Under identical input data, medium- and long-term strategies, and training conditions, it compares joint renewable-storage operation and independent participation. Evaluation covers training convergence, operating profit, consumer procurement cost, contract performance, renewable curtailment, and storage operation. The case study shows that joint operation can increase profit and reduce curtailment by coordinating renewable output with storage charging and discharging, balancing system economics and consumer cost.

The remainder of this study is organized as follows. Section 2 introduces the multi-timescale electricity-market structure and formulates bidding and clearing models for generation, medium- and long-term trading, and real-time trading. Section 3 develops the WoLF-PHC multi-agent bidding model, including the state spaces, action spaces, reward functions, and solution procedure for demand- and generation-side agents. Section 4 evaluates training stability, economic performance, and renewable integration through a case study, participation-mode comparisons, and storage energy–power sensitivity analyses. Section 5 summarizes the main findings, limitations, and directions for future work.

2. Market Structure and Market Participant Bidding Model

Modern electricity energy markets span medium- and long-term trading and day-ahead, intraday, and real-time operation. Medium- and long-term markets cover annual, monthly, and weekly transactions; forward contracts are concluded through bilateral negotiation or centralized bidding to lock in energy and prices, mitigate exposure risk, and stabilize generators' baseline revenues. In the day-ahead spot market, generators submit piecewise price–quantity bids, and joint security-constrained unit commitment and security-constrained economic dispatch determine generation schedules and locational marginal prices. The intraday market updates day-ahead deviations on a rolling basis, while the real-time market performs final balancing every 15 (or 5) min. Real-time price fluctuations reflect system scarcity and reward flexible resources. These four layers provide the broader market context. To focus on electricity energy market simulation using artificial intelligence, the proposed model adopts a basic centralized pool framework without transmission constraints [38]. Clearing is represented as a uniform-price auction, allowing analysis of participants' intertemporal bidding strategies and coordinated returns.

2.1. Analysis of Market Structure

The electricity energy market architecture developed in this study comprises monthly and weekly medium- and long-term markets, day-ahead and intraday spot markets, and a real-time market operating at 15 min intervals. This architecture supports analysis of electricity-market participants' bidding decisions across multiple time scales.

The medium- and long-term market is centered on monthly contracts, supplemented by weekly transactions. Generators and consumers enter financially settled energy contracts through centralized bidding, with a one-month contract period. This market layer locks in baseline prices and supply for most electricity, mitigates spot-price risk, and stabilizes expected generator revenue. Medium- and long-term contracts typically cover 70–90% of total consumer demand.

The day-ahead market uses next-day load and renewable-output forecasts. Participants submit hourly bids, which are mapped to 96 15 min intervals for joint clearing to determine awarded energy, prices, and baseline operating schedules. Forecast renewable output enters the agent state and informs bidding and scheduled delivery. Storage schedules account for SOC and charging and discharging constraints across intervals. Day-ahead bid prices and bid-block capacity boundaries are frozen at gate closure.

At each hour, the intraday stage updates the remaining operating schedule using revised load and renewable-output forecasts. Participants select available capacity and charging or discharging intentions according to updated forecasts and actual equipment states. These decisions adjust the day-ahead schedule within physical limits and provide dispatchable limits and reference values for terminal energy for real-time execution. Intraday operation neither resubmits prices nor introduces a separate energy-settlement layer.

The real-time market performs rolling optimization at 15 min intervals using ultra-short-term load and renewable-output forecasts and actual unit operating states. Actual output is revealed after action selection and enters feedback rebalancing as the available power for the current interval. Physical clearing and storage charging and discharging address forecast errors. Remaining surplus energy is counted as curtailment, while delivery below the published real-time schedule is assessed as a shortfall. Revenues and penalties enter agent rewards, allowing policies to learn trade-offs among forecast errors, storage states, and market prices.

Contract-energy decomposition and deviation settlement couple the two market layers. The market operator decomposes medium- and long-term contract energy progressively into 15 min intervals, producing a reference contract quantity (MWh) for each participant and interval. Deviation settlement compares real-time cleared output with this reference quantity and applies a prescribed penalty coefficient to the deviation. This mechanism encourages truthful contract declarations and contract performance.

Renewable-output uncertainty is represented using separate forecast and actual-output series. Forecast output enters the agent state and informs bidding and scheduled delivery, whereas actual output sets the real-time availability limit for clearing and settlement. Storage charging and discharging first balance the forecast error within each plant; remaining surplus energy is treated as renewable curtailment, and delivery shortfalls are included in deviation assessment. The resulting revenue and penalties enter the agent reward, allowing the bidding policy to learn the trade-off among forecast error, storage state, and market price.

To constrain favorable price-difference gains arising from contract deviations, this study introduces a periodic K-recovery mechanism based on the 2024 continuous trial-operation plan for the southern Hebei electricity spot market [39]. The plan was issued by the Hebei Provincial Development and Reform Commission and specifies allowable-range parameters of 90 and 110 and an adjustment factor of 1.05. The simulation adopts this regulatory approach and these parameter values, defines performance as actual energy divided by

contract energy, and adapts the accumulation window. This study defines one cycle as 24 h, or 96 15 min intervals, and calculates the performance rate as cumulative actual settled energy divided by cumulative contract energy. The allowable band is 90–110%. When the rate is below 90% and the contract price exceeds the cycle-average real-time price, the favorable price-difference revenue associated with the under-delivered energy is recovered using a multiplier of 1.05. When the rate exceeds 110% and the cycle-average real-time price exceeds the contract price, excess-contract revenue is recovered using the same multiplier. No recovery is applied when performance remains within the band or the price difference is unfavorable. During training, the interval increment in cumulative K-recovery amount provides feedback; final settlement uses the cumulative K-recovery amount at the end of the cycle.

This multi-timescale architecture coordinates medium- and long-term risk hedging with short-term flexibility through market organization and economic signals. It is particularly suitable for power systems with high shares of renewable generation. The resulting multi-timescale electricity energy market architecture is illustrated in Figure 1.

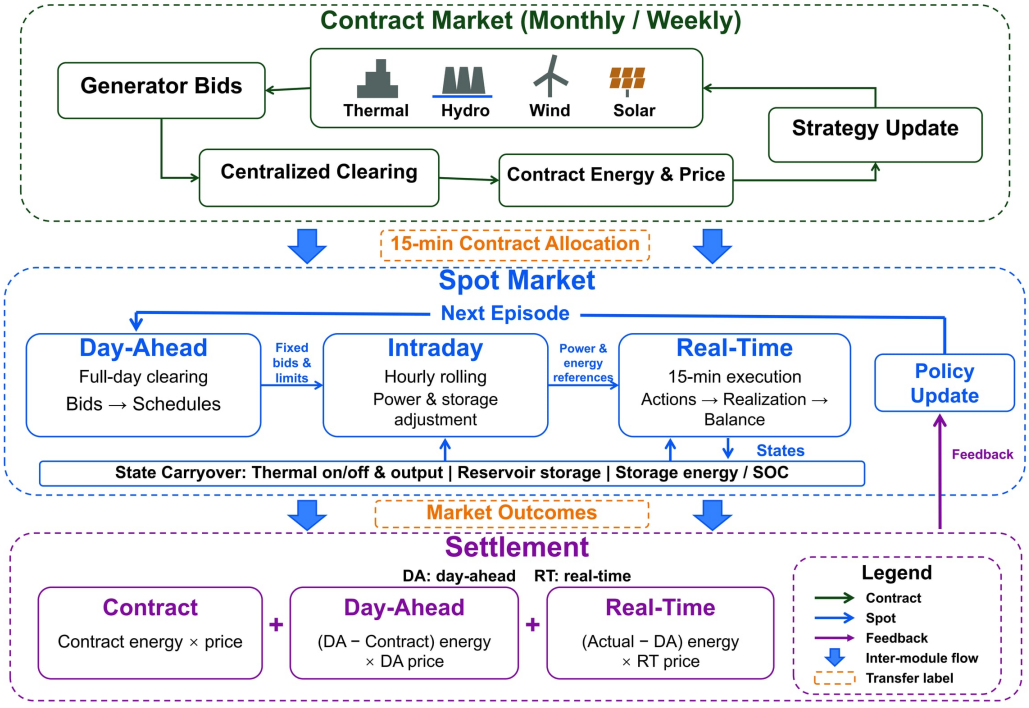


Figure 1. Electricity energy market architecture.

2.2. Market Participant Bidding Model

The participant bidding models represent the decisions and profit objectives of each actor across the market layers. First, generation-side units submit piecewise bids to maximize profit. The centralized bidding and marginal-clearing model for the medium- and long-term market then determines energy contracts. Finally, economic dispatch subject to unit operating constraints is introduced in the day-ahead, intraday, and real-time stages to determine schedules and actual output that maintain system balance.

2.2.1. Generation-Side Unit Bidding Model

Generation-side participants include thermal, hydropower, wind, photovoltaic, and storage units. Each unit bids to maximize its own profit, and the generic objective function is expressed as follows:

$$\max R_i^{net} = R_i - C_i \quad (1)$$

where R_i^{net} is the net revenue of generating unit i, R_i is its energy-market revenue, and C_i is its cost.

Generation cost is a primary determinant of generation-side bidding. Because cost structures differ substantially across technologies, this section formulates representative cost models for thermal power, hydropower, and renewable plants equipped with storage.

(1) Thermal unit:

$$C_{thermal} = C^{fix} + C^{start/stop} \cdot u^{su} + aP^2 + bP \quad (2)$$

where $C_{thermal}$ is total thermal-generation cost in the interval; C^{fix} is fixed operation and maintenance cost, expressed in CNY 10,000/year and allocated to the interval; $C^{start/stop}$ is the cost per start-up or shutdown event, expressed in CNY 10,000/event; and u^{su} is the binary start-up indicator. Parameters a and b are fuel-cost coefficients fitted to the marginal costs at minimum and rated output. P is unit output (MW).

(2) Hydropower unit:

$$C_{h,t} = C_{h,t}^{fix}, P_{h,t} = \kappa_h q_{h,t} \quad (3)$$

Only fixed operation and maintenance costs are considered for hydropower. Subscript h denotes a hydropower unit; t and t + 1 denote consecutive dispatch intervals. The interval duration is Δt (h), and T denotes the end of the complete scheduling horizon. To represent intertemporal water-use constraints, effective head and unit efficiency are approximated as constant over the horizon. An equivalent conversion coefficient links power output to turbine flow, subject to the following water balance:

$$V_{h,t+1} = V_{h,t} + 3600\Delta t(I_{h,t} - q_{h,t} - s_{h,t}) \quad (4)$$

$$V_h^{min} \le V_{h,t} \le V_h^{max}, 0 \le q_{h,t} \le q_h^{max}, s_{h,t} \ge 0 \quad (5)$$

$$V_{h,0} = V_h^{ini}, V_{h,T} \ge V_h^{tar} \quad (6)$$

Here, $C_{h,t}$ and $C_{h,t}^{fix}$ are interval generation cost and fixed operation and maintenance cost (CNY), respectively. $P_{h,t}$ is hydropower output (MW), and κ_h is the equivalent conversion coefficient [MW/(m^3/s)]. $V_{h,t}$ is reservoir volume at the interval start (m^3), bounded by V_h^{min} and V_h^{max}. $I_{h,t}$, $q_{h,t}$, and $s_{h,t}$ denote inflow, turbine flow, and spillage (m^3/s), respectively; q_h^{max} is the maximum turbine flow. V_h^{ini} and V_h^{tar} denote initial volume and the minimum terminal reserve. The factor 3600 converts hours to seconds. Initial volume and terminal reserve jointly limit water available for generation; intraday and real-time optimization inherit actual reservoir volume.

(3) Renewable plant (wind or photovoltaic generation plus storage):

$$C_{re} = C^{fix} + C_{ch} + C_{dis} \quad (7)$$

where C^{fix} is the fixed cost. Let the actual renewable output of the plant in interval t be $P_t^{RE,actual}$ (MW), and let its awarded output from market clearing be $P_t^{RE,bid}$ (MW). When $P_t^{RE,bid} < P_t^{RE,actual}$, storage can absorb the surplus generation, incurring charging cost C_{ch}; when $P_t^{RE,bid} > P_t^{RE,actual}$, storage must discharge to cover the delivery shortfall, incurring discharging cost C_{dis}.

Charging cost C_{ch}: when storage charges at power $P_{ch}(t)$ for duration Δt, the charged energy is $E_{ch} = P_{ch}(t)\Delta t$ (MWh). Charging cost includes the variable storage-use cost and the energy-loss cost caused by charging inefficiency:

$$C_{ch} = c_{sto} \cdot E_{ch} + \left(1 - \eta_{ch}\right) \cdot p_{ch} \cdot E_{ch} \quad (8)$$

where

c_{sto} is the variable operating cost of the energy-storage system (CNY/MWh), including depreciation, operation, and maintenance costs; η_{ch} is the charging efficiency ($0 < \eta_{ch} < 1$), defined as the ratio of energy stored in the battery to charging input energy; p_{ch} is the market electricity price during charging (CNY/MWh); this term represents the additional procurement cost caused by charging losses; $(1-\eta_{ch}) \cdot E_{ch}$ is the charging energy loss (MWh).

The charging-cost function can therefore be written as:

$$C_{ch} = c_{sto} \cdot E_{ch} + \frac{1-\eta_{ch}}{\eta_{ch}} \cdot p_{ch} \cdot E_{ch,out} \quad (9)$$

where $E_{ch,out} = \eta_{ch} E_{ch}$ is the energy effectively stored in the battery.

Discharging cost C_{dis}: when storage discharges at power $P_{dis}(t)$ for duration Δt, the delivered energy is $E_{dis,out} = P_{dis}(t)\Delta t$ (MWh). Because the discharging efficiency is η_{dis}, the battery must release $E_{dis,actual} = E_{dis,out}/\eta_{dis}$ (MWh). The discharging cost comprises the variable storage-use cost and the cost associated with discharge losses:

$$C_{dis} = c_{sto} \cdot E_{dis,actual} + \left(\frac{1}{\eta_{dis}} - 1\right) \cdot p_{dis} \cdot E_{dis,out} \quad (10)$$

where p_{dis} is the market electricity price during discharge (CNY/MWh), and $\left(\frac{1}{\eta_{dis}} - 1\right) E_{dis,out}$ is the energy loss during discharge (MWh).

2.2.2. Medium- and Long-Term Market Clearing Model

The medium- and long-term market primarily trades energy contracts through centralized bidding and marginal clearing. The monthly and weekly markets are modeled as one-sided procurement auctions. Each generator submits a three-block supply bid, while consumer demand is fixed. The clearing objective minimizes the sum of procurement cost and the load-shedding slack penalty:

Objective function:

$$\min \sum_{j \in \mathcal{G}} \rho_j E_j + \sigma_{short} E^{short} \quad (11)$$

where $\mathcal{G}$ is the set of generators, $\mathcal{L}$ is the set of consumers; ρ_j is generator j's submitted bid (CNY/MWh); E_j is its cleared contract energy (MWh); σ_{short} is the load-shedding penalty coefficient; and E^{short} is the load-shedding slack variable.

Constraints:

(1) Energy-balance constraint:

$$\sum_j E_j + E^{short} = E^{demand} \quad (12)$$

(2) Bid-block quantity constraint: the awarded quantity in each bid block cannot exceed the declared capacity of that block.

$$0 \le E_{j,b} \le E_{j,b}^{max}, \forall j, b \quad (13)$$

(3) Total-energy constraint: each participant's total cleared contract energy cannot exceed its declared quantity limit.

$$0 \le E_j \le E_j^{bid} \quad (14)$$

(4) Clearing price: under the single-node uniform marginal-clearing mechanism, the market-clearing price (MCP) is the dual variable of the energy-balance constraint. It represents the incremental optimal procurement cost associated with a 1-MWh increase

in market demand. When supply is sufficient and the shortage slack variable is zero, the MCP equals the price of the marginal accepted bid block. When the declared supply is insufficient and the shortage slack variable is positive, the MCP is set by the shortage-penalty price.

$$\mathrm{MCP}^{\mathrm{LT}} = \lambda^{\mathrm{LT}}_{\mathrm{balance}} = \begin{cases} \rho_{j^*,b^*} & \text{if} E^{\mathrm{short}} = 0 \\ \sigma_{\mathrm{short}} & \text{if} E^{\mathrm{short}} > 0 \end{cases} \tag{15}$$

where $\lambda^{\mathrm{LT}}_{\mathrm{balance}}$ is the dual variable of the medium- and long-term energy-balance constraint. The symbols j* and b* denote the marginal generator and its marginal bid block, respectively. ρ_{j^*,b^*} is the bid price of that block (CNY/MWh).

2.2.3. Day-Ahead Market Clearing Model

The medium- and long-term stage is denoted by LT; DA, ID, and RT denote day-ahead, intraday, and real-time stages, respectively. Day-ahead clearing uses next-day load and renewable-output forecasts and maps participants' frozen hourly piecewise bids to 96 15 min intervals. It jointly determines unit commitment, awarded output, and storage charging and discharging schedules. Decomposed contract energy serves as the settlement position. Clearing minimizes bid cost, thermal minimum-output operating and start-up/shutdown costs, storage-use cost, and supply-demand slack penalties.

Objective function: superscript s denotes a spot-market stage, taking DA, ID, or RT. J^{DA} is the full-day objective (CNY), and T^{DA} contains all 96 next-day dispatch intervals. The interval objective and its cost components are defined consistently across stages:

$$minJ^{DA} = \sum\nolimits_{t\in \mathcal{T}^{DA}} L_t^{DA} \tag{16}$$

$$L_t^s = \Delta t(A_t^s + B_t^s + C_t^s + \pi_{short}\ell_t^s + \pi_{excess}x_t^s) + S_t^s \tag{17}$$

$$A_t^s = \sum\nolimits_{j\in G}\sum\nolimits_{b}\rho_{j,b,h(t)}\, P_{j,b,t}^s,\ B_t^s = \sum\nolimits_{g\in G_{th}} B_g\, u_{g,t}^s \tag{18}$$

$$C_t^s = \sum\nolimits_{k\in K}(c_{ch,k}P_{ch,k,t}^s + c_{dis,k}P_{dis,k,t}^s) \tag{19}$$

$$S_t^s = \sum\nolimits_{g\in G_{th}}(C_g^{start}y_{g,t}^s + C_g^{stop}z_{g,t}^s) \tag{20}$$

The terms A, B, and C are the rates of bid cost, thermal minimum-output operating cost, and associated storage-use cost (CNY/h), respectively. S is interval start-up/shutdown cost (CNY), and L is measured in CNY. G denotes generators; Gth denotes thermal units, and K denotes storage associated with renewable plants. Indices j, g, k, and b denote generators, thermal units, storage-owning plants, and bid blocks, respectively. The bid-hour mapping h(t) is distinct from the hydropower-unit index h. The frozen block price $\rho_{j,\beta,h(t)}$ is in CNY/MWh, and the awarded block output P is in MW. Thermal bid blocks represent increments above minimum technical output. B_g is minimum-output operating cost (CNY/h); u, y, and z are binary online, start-up, and shutdown variables. C_g^{start} and C_g^{stop} are event costs (CNY). Variables l and x represent supply shortage and forced system surplus (MW), with penalties π_{short} and π_{excess} (CNY/MWh). Here, $\Delta t = 0.25$ h. Shared constraints below omit stage superscripts and retain these definitions.

Constraints:

(1) System power balance:

$$\sum\nolimits_{j\in G}P_{j,t} - x_t + \ell_t = D_t, x_t \geq 0, 0 \leq \ell_t \leq D_t \tag{21}$$

Here, $P_{j,t}$ denotes thermal or hydropower generation, or net renewable-plant delivery (MW), and D_t is the corresponding stage's load forecast (MW). Associated storage charging is deducted from plant net delivery and is not added again to system load.

(2) Bid-block output and declared-capacity constraints:

$$0 \le P_{j,b,t} \le P_{j,b} u_{j,t}, P_{j,t} = P_j^{min} u_{j,t} + \sum\nolimits_b P_{j,b,t}, j \in G_{th} \quad (22)$$

$$0 \le P_{j,b,t} \le P_{j,b}, P_{j,t} = \sum\nolimits_b P_{j,b,t}, j \in G \setminus G_{th} \quad (23)$$

Here, $\overline{P}_{j,b}$ is declared block capacity (MW). Thermal blocks represent increments above minimum output; other participants' blocks represent delivery capacity. P_j^{min} is minimum thermal output (MW). The set difference G\Gth contains all non-thermal generators.

(3) Unit-output and water-volume limits:

$$P_g^{min} u_{g,t} \le P_{g,t} \le P_g^{max} u_{g,t}, 0 \le P_{h,t} \le P_h^{max} \quad (24)$$

Here, P_g^{max} and P_h^{max} are rated thermal and hydropower output limits (MW), respectively. Other symbols retain their definitions and are distinguished by unit indices. Thermal output depends on commitment status; hydropower also satisfies Equations (3)–(6).

(4) Ramping between consecutive intervals:

$$P_{g,t} - P_{g,t-1} \le R_g^{up} \Delta t u_{g,t-1} + S_g^{up} y_{g,t} \quad (25)$$

$$P_{g,t-1} - P_{g,t} \le R_g^{down} \Delta t u_{g,t} + S_g^{down} z_{g,t} \quad (26)$$

$$-R_h^{down} \Delta t \le P_{h,t} - P_{h,t-1} \le R_h^{up} \Delta t \quad (27)$$

Superscripts up and down denote upward and downward changes. R_g^{up}, R_g^{down}, R_h^{up}, and R_h^{down} are nonnegative thermal and hydropower ramp rates (MW/h). S_g^{up} and S_g^{down} are allowable thermal start-up and shutdown power changes (MW). The first interval inherits actual output and commitment from the preceding interval. Start-up and shutdown allowances are treated separately from normal online ramping.

(5) Thermal commitment logic and minimum up/down times:

$$u_{g,t} - u_{g,t-1} = y_{g,t} - z_{g,t}, y_{g,t} + z_{g,t} \le 1 \quad (28)$$

$$\sum\nolimits_{r=t-U_g+1}^{t} y_{g,r} \le u_{g,t}, \sum\nolimits_{r=t-D_g+1}^{t} z_{g,r} \le 1 - u_{g,t} \quad (29)$$

Here, U_g and D_g are the minimum up and down times divided by Δt and rounded upward to interval counts. The summation index r denotes an interval, rather than the rolling origin used later. Known start-up/shutdown histories supply states preceding the scheduling origin. Units whose initial continuous online or offline duration is insufficient retain their original status for the remaining mandatory intervals.

(6) Associated storage and renewable-plant constraints:

$$SOC_k^{min} \le SOC_{k,t} \le SOC_k^{max}, E_{k,t} = E_k^{rated} SOC_{k,t} \quad (30)$$

$$0 \le P_{ch,k,t} \le P_{ch,k}^{max} v_{k,t}, 0 \le P_{dis,k,t} \le P_{dis,k}^{max} (1 - v_{k,t}), v_{k,t} \in \{0,1\} \quad (31)$$

$$P_{k,t} + P_{ch,k,t} + P_{curt,k,t} = \hat{P}_{RE,k,t} + P_{dis,k,t} \quad (32)$$

$$0 \le P_{ch,k,t} + P_{curt,k,t} \le \hat{P}_{RE,k,t}, P_{curt,k,t} \ge 0, 0 \le P_{k,t} \le P_k^{grid,max} \quad (33)$$

Storage energy is updated by adding efficiently stored charging energy and subtracting discharge energy adjusted for discharge efficiency. SOC is stored energy divided by rated energy capacity and is expressed as a ratio or percentage. SOC^{min} and SOC^{max} are its bounds; P_{ch}^{max} and P^{dismax} are charging and discharging limits (MW). The binary variable v permits charging when equal to 1 and discharging when equal to 0. $\hat{P}_{RE}$ denotes forecast available renewable power, with a hat indicating a forecast. P_c^{urt} denotes ordinary curtailment, and $P_g^{rid,max}$ is the plant grid-delivery limit, all in MW. Associated storage charges are only from its own renewable plant, cannot purchase grid electricity, and cannot charge and discharge simultaneously.

(7) Day-ahead initial and terminal storage conditions:

$$E_{k,0}^{DA} = E_k^{ini}, E_{k,T}^{DA} = E_k^{ini} \tag{34}$$

Here, E_k^{ini} is the initial storage energy at the start of the complete operating day (MWh). Equal initial and terminal energy prevents day-ahead profit from being obtained by depleting inventory. Clearing determines day-ahead energy awards, commitment, and intertemporal energy schedules. With integer decisions fixed, day-ahead prices are derived from power-balance dual values and adjusted by Δt. Supply–demand slack triggers a fallback rule based on accepted bids.

2.2.4. Intraday Market Clearing Model

At each hour, intraday operation reoptimizes all remaining intervals through day-end using updated load and renewable-output forecasts. Frozen day-ahead bids remain in force, without separate intraday energy settlement. The resulting physical adjustment schedule provides dispatchable-power limits and storage-energy references for real-time operation.

Objective function:

$$minJ^{ID}(\tau) = \sum\nolimits_{t \in T^{ID}(\tau)} L_t^{ID} + \sum\nolimits_{k \in K} \mu_k d_k^{ID} \tag{35}$$

Here, τ is the current rolling origin, and $T^{ID}(\tau)$ contains all remaining dispatch intervals before day-end. $J^{ID}(\tau)$ is the intraday objective (CNY). Interval costs follow Equation (17), with updated forecasts and initial states. The auxiliary variable d^{ID} bounds absolute terminal-energy deviation from the storage target (MWh); μ_k is a positive penalty coefficient (CNY/MWh).

Constraints: intraday clearing inherits power balance, bid-capacity, unit-output, ramping, commitment, and storage constraints in Equations (21)–(33), using updated forecasts. Hydropower inherits actual reservoir volume under Equations (3)–(6). At the rolling origin, executed states replace day-ahead forecast states:

$$E_{k,\tau}^{ID} = E_{k,\tau}^{actual}, V_{h,\tau}^{ID} = V_{h,\tau}^{actual}, P_{j,\tau-1}^{ID} = P_{j,\tau-1}^{actual} \tag{36}$$

Superscript actual denotes executed states. $E_{k,\tau}^{actual}$ and $V_{h,\tau}^{actual}$ are actual storage energy and reservoir volume at the rolling origin; $P_{j,\tau_{-1}}^{actual}$ is preceding actual output. Thermal commitment and continuous online/offline durations are also inherited. Subsequent commitment may be adjusted within physical limits, with day-ahead commitment serving as a reference.

The strict day-ahead terminal-energy equality in Equation (34) is replaced during rolling optimization by:

$$d_k^{ID} \geq E_{k,T}^{ID} - E_k^{tar}, d_k^{ID} \geq E_k^{tar} - E_{k,T}^{ID}, d_k^{ID} \geq 0 \tag{37}$$

Here, E_k^{tar} is the full-day terminal-energy target (MWh), equal to initial day-ahead energy. Equation (37) bounds the auxiliary variable below by the absolute energy difference. Its positive penalty coefficient makes it equal that difference at optimality. This soft terminal target encourages inventory recovery. Charging and discharging are additionally limited by dispatchable fractions selected in the current operating decision:

$$P_{ch,k,t} \leq \alpha_{ch,k,t}^{ID} P_{ch,k}^{max}, P_{dis,k,t} \leq \alpha_{dis,k,t}^{ID} P_{dis,k}^{max}, 0 \leq \alpha_{ch,k,t}^{ID}, \alpha_{dis,k,t}^{ID} \leq 1 \tag{38}$$

Here, α_{ch}^{ID} and α^{disID} are selected charging and discharging fractions, both dimensionless and between 0 and 1. Thermal operating decisions limit dispatchable increments above minimum technical output; hydropower decisions limit dispatchable output. These limits must accommodate actual initial output and downward-ramping capability. Intraday schedules do not change frozen day-ahead financial positions.

2.2.5. Real-Time Market Clearing Model

Real-time operation optimizes a rolling window at 15 min execution intervals using ultra-short-term forecasts and current equipment states, executing only the first interval. Actual load and renewable output are revealed after operating-action selection. Feedback balancing under the same physical constraints then determines actual delivered energy. Frozen bids remain in force, and intraday decisions additionally constrain dispatchable power.

Objective function:

$$minJ^{RT}(\tau) = \sum_{t\in T^{RT}(\tau)} L_t^{RT} + \sum_{k\in K} \mu_k d_k^{RT} \quad (39)$$

Here, $J^{RT}(\tau)$ is the real-time objective (CNY), and $T^{RT}(\tau)$ contains intervals in the current rolling window. The auxiliary variable d^{RT} bounds absolute terminal-energy deviation from the intraday reference (MWh). Other symbols and cost components retain their definitions. Real-time operation uses Equations (21)–(33), initialized with the latest actual states as in Equation (36). After action selection, actual values replace load and renewable forecasts for the first interval; subsequent intervals retain forecasts. The terminal storage reference is taken from the intraday schedule:

$$d_k^{RT} \geq E_{k,H}^{RT} - E_{k,H}^{ID}, d_k^{RT} \geq E_{k,H}^{ID} - E_{k,H}^{RT}, d_k^{RT} \geq 0 \quad (40)$$

Here, H is the current real-time window endpoint. $E_{k,H}{}^{RT}$ and $E_{k,H}{}^{ID}$ denote optimized real-time and reference intraday energy at that endpoint, respectively (MWh). Charging and discharging are subject to hierarchical intraday and real-time dispatchable limits in the form of Equation (38). Intraday commitment may initialize the real-time solution, while real-time commitment remains subject to initial states, minimum durations, and ramping constraints.

Supply-shortage and forced-surplus slack variables maintain feasibility under extreme conditions. Ordinary renewable curtailment is accounted for separately in Equations (32) and (33). Normally, uniform marginal prices are derived from power-balance dual values after integer decisions are fixed. If rolling optimization uses supply-demand slack, the highest valid accepted bid provides fallback pricing, preventing slack-penalty coefficients from directly setting market prices. Actual delivery enters real-time difference settlement; intraday operation has no separate energy cash flow. Delivery-shortfall penalties and periodic K-recovery are calculated separately.

3. Market Bidding Model and Multi-Agent Reinforcement-Learning Approach

Electricity markets are complex systems of heterogeneous generators, consumers, and storage operators. Each participant makes independent profit-oriented decisions and interacts strategically under renewable uncertainty and coordination across multiple time scales, producing high-dimensional, dynamic, and non-stationary behavior. Conventional centralized optimization assumes complete information; Nash-equilibrium analysis faces the curse of dimensionality; and single-agent reinforcement learning struggles with a non-stationary environment. Multi-agent reinforcement learning instead represents the market as a distributed system in which participants learn adaptive bidding policies from local observations and approach an equilibrium, making it well suited to strategic market interactions.

3.1. Multi-Agent Reinforcement-Learning Market Bidding Model

To integrate multi-agent reinforcement learning with market bidding, the operating constraints of thermal power, hydropower, renewable generation, and storage are embedded in the environment response to agent actions. The state space, action space, and reward

functions of the resulting multi-agent model are defined below. Figure 2 shows how the heterogeneous agents interact with the market environment through states, actions, clearing outcomes, and rewards.

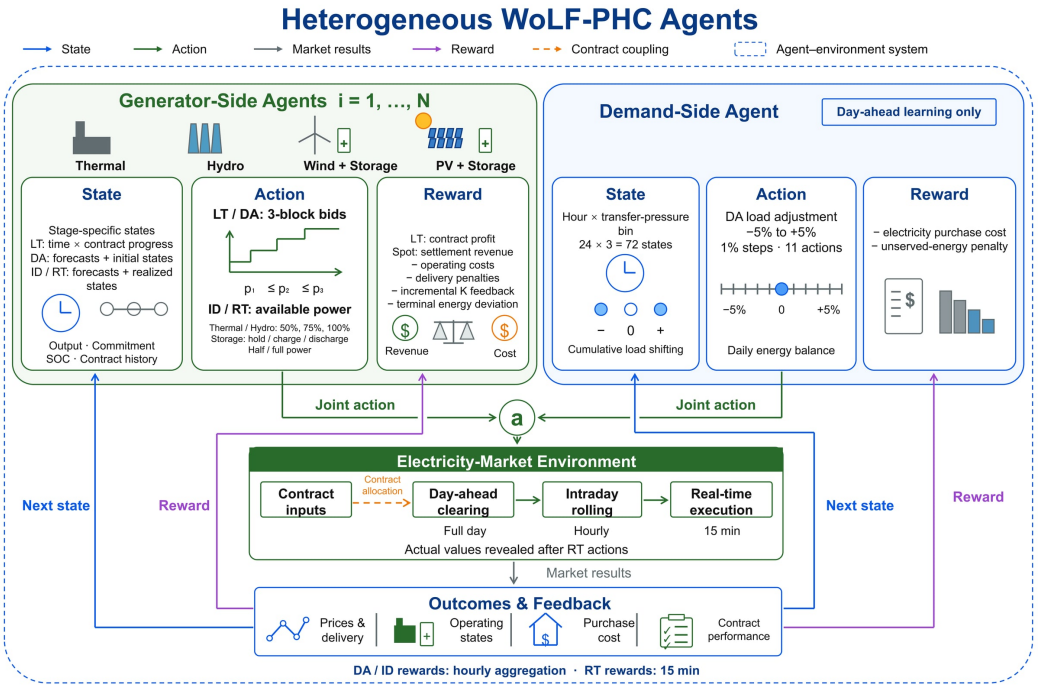


Figure 2. Agent architecture.

3.1.1. Demand-Side Agent Bidding Model

A demand-side participant, such as an electricity retailer or large consumer, is modeled as an agent that minimizes procurement cost. Consumers do not learn medium- and long-term strategies. In the spot market, they select hourly day-ahead load-adjustment ratios. Intraday and real-time operation maintain energy balance over the remaining horizon using updated forecasts and executed purchases.

(1) State Space

Consumers submit quantities rather than prices. The day-ahead state combines the bid hour with a cumulative load-shifting pressure level. Its state set and elements are defined as:

$$\mathcal{S}_u^{DA} = \mathcal{T}^{DA} \times \mathcal{L}_u, \quad s_{u,h}^{DA} = (h, \ell_{u,h}) \tag{41}$$

Here, S_u^{DA} is the consumer day-ahead state set; $T^{DA} = \{0, \ldots, 23\}$ is the set of bid hours, with h denoting one hour. $L_u = \{0, 1, 2\}$ contains cumulative load-shifting pressure levels. The level $l_{u,h}$ indicates cumulative downward adjustment, approximate balance, or cumulative upward adjustment, respectively. The state $s_{u,h}^{DA}$ combines h and $l_{u,h}$. Subscript u denotes the consumer, superscript DA denotes day-ahead operation, and × denotes the Cartesian product. The discrete day-ahead state set therefore contains $24 \times 3 = 72$ combinations.

The pressure level compares cumulative scheduled energy shifting with remaining adjustable energy, representing the difficulty of restoring full-day consumption balance. During execution, the cumulative deviation of actual purchases from baseline demand continues to be recorded:

$$D_{u,t} = D_{u,t-1} + \left(P_{u,t}^0 - P_{u,t}^a\right)\Delta t \tag{42}$$

where $P_{u,t}^0$ is consumer baseline load, $P_{u,t}^a$ is actual purchased power, and $D_{u,t} > 0$ is cumulative under-purchase through interval t. To represent the difficulty of eliminating

this cumulative deviation over the remaining horizon, the required average correction ratio for the next interval is defined as

$$z_{u,t+1} = \frac{D_{u,t}}{E^{rem}_{u,t+1}} \tag{43}$$

The denominator in Equation (42) is the remaining baseline consumption from the next interval through the end of the horizon. Equations (41) and (42) describe the executed cumulative deviation and its relative magnitude. At day-ahead submission, cumulative energy shifting before the current hour is divided by adjustable energy in the current and subsequent intervals. Pressure below $-1/3$, between $-1/3$ and $1/3$ inclusive, and above $1/3$ is assigned to levels 0, 1, and 2, respectively. Each hour, the consumer chooses a feasible load adjustment from -5% to 5% at one-percentage-point intervals. The final hour eliminates remaining energy shifting. Intraday and real-time operation retain the day-ahead shifting schedule, with remaining-energy feasibility corrections when necessary, rather than learning a separate consumer bidding policy.

(2) Action Space

Day-ahead submission: the action is the adjustment ratio relative to baseline demand, with 11 candidate levels from -5% to 5% in one-percentage-point increments. Before selection, candidates that prevent full-day balance from being restored within remaining adjustment limits are removed. The final-hour adjustment is determined by remaining energy. Actual procurement costs and deviation feedback evaluate the day-ahead submission policy.

(3) Immediate Reward

The consumer day-ahead policy is evaluated using actual procurement expenditure and unserved-energy feedback:

$$r_{u,t} = -C^{buy}_{u,t} - \lambda_u q^{unserved}_{u,t} \tag{44}$$

$$C^{buy}_{u,t} = C^{LT}_{u,t} + (q^{DA}_{u,t} - q^{LT}_{u,t})\lambda^{DA}_t + (q^{act}_{u,t} - q^{DA}_{u,t})\lambda^{RT}_t \tag{45}$$

Consumer purchases are positive. C^{buy} denotes procurement expenditure calculated from medium- and long-term, day-ahead, and real-time energy differences. Unserved energy is denoted by $q^{unserved}$, with $\lambda_u = 1500$ CNY/MWh. The day-ahead policy receives hourly sums of executed rewards. Consumer compensation surcharges enter the final settlement bill.

3.1.2. Generation-Side Agent Bidding Model

Each generator is modeled as an agent that maximizes its profit in every trading cycle. By interacting with the market environment, including other generators, consumers, and the system operator, the generator learns to select an optimal bid curve.

(1) State Space

Generator states combine stage-specific decision times with participant characteristics. Medium- and long-term states reflect contracting progress. Day-ahead states use information available before bid freezing: load and renewable forecasts, initial equipment states, and historical contract performance. Intraday and real-time states update with revised forecasts and executed outcomes. Each stage uses only information available at its decision time.

For the medium- and long-term market, the state set is the Cartesian product of trading-time and contracting-progress sets:

$$\mathcal{S}^{LT}_i = \mathcal{T}^{LT} \times \mathcal{K}_i, \;\; s^{LT}_i = (w, k) \tag{46}$$

Here, S_i^{LT} is generator i's medium- and long-term state set; T^{LT} is the trading-time set, and w denotes the trading week. K_i contains contracting-progress levels, with k denoting a

level. The state s_i^{LT} combines w and k. Subscript i denotes the generator, superscript LT denotes the medium- and long-term stage, and × denotes the Cartesian product.

Contract-signing progress k has seven levels. Level 0 denotes no contract; levels 1 and 2 denote partial and complete contracting of bid block 1; levels 3 and 4 apply to bid block 2; and levels 5 and 6 apply to bid block 3. The total number of medium- and long-term market states is therefore $4 \times 7 = 28$.

For the day-ahead, intraday, and real-time stages, state sets and their elements are written consistently as:

$$\mathcal{S}_i^s = \mathcal{T}^s \times \Xi_i^s, \;\; s_{i,\tau}^s = (\tau, \xi_{i,\tau}^s), \;\; s \in \{DA, ID, RT\} \tag{47}$$

Here, S_i^s is generator i's state set in stage s; T^s is that stage's decision-time set, and τ is a decision time. Ξ_i^s contains participant features; $\xi_{i,\tau}^s$ is the discrete feature vector at τ. The state $s_{i,\tau}^s$ combines τ and that vector. Stage s takes DA, ID, or RT. Day-ahead and intraday decisions are hourly, while real-time decisions occur at 15 min intervals. Table 1 lists participant feature vectors, and Table 2 defines their symbols and discretization.

Table 1. Participant state-feature vectors by market stage.

Participant	Day-Ahead Feature Vector	Intraday and Real-Time Feature Vector
Thermal	$\xi_i^{DA} = (n, c_i, f_i)$	$\xi_i^s = (p_i, c_i, n)$
Hydropower	$\xi_i^{DA} = (n, p_i, f_i)$	$\xi_i^s = (p_i, n)$
Renewable-storage	$\xi_i^{DA} = (b_i, z_i, n, f_i)$	$\xi_i^s = (z_i, b_i, n, g_i)$

Table 2. State-feature definitions and discretization.

Symbol	Definition	Discretization and Values
n	Net-load level	Forecast load minus forecast renewable output, normalized by total rated thermal and hydropower capacity; low, medium, and high levels.
p_i	Output-ratio level	Boundaries at 1/3 and 2/3 of rated capacity. Use output at bid submission for the day-ahead stage and preceding actual output for the intraday and real-time stages.
c_i	Commitment-duration level	Day-ahead: initial commitment and satisfaction of minimum duration. Intraday/real-time: current commitment and remaining minimum duration, classified as satisfied, at most 1 h, or more than 1 h.
f_i	Historical contract-performance level	Underperformance, normal performance, and overperformance, bounded by 90% and 110%.
b_i	Forecast surplus/shortfall level	Forecast renewable output minus decomposed contract power, normalized by rated renewable capacity; boundaries at −2.5% and 2.5%.
z_i	SOC level	Boundaries at 1/3 and 2/3. Use SOC at bid submission for the day-ahead stage and current SOC for the intraday and real-time stages.
g_i	Storage energy deviation level	Current energy minus terminal reference energy, normalized by rated energy; boundaries at −10% and 10%.

(2) Action Space

In the medium- and long-term and day-ahead stages, a generator's action is a non-decreasing three-block stepwise bid curve. Block capacities are fixed, while prices are adjustable. Each block's admissible range is discretized into M price points, which are combined in non-decreasing order to form the bid-curve set.

Medium- and long-term market: let the minimum bid be $P_{\min}^{\mathrm{LT}}$, the maximum bid be $P_{\max}^{\mathrm{LT}}$, and the discretization step be ΔP^{LT}. The number of valid price points is $\mathrm{M}^{\mathrm{LT}} = \frac{\mathrm{P}_{\max}^{\mathrm{LT}} - \min}{\Delta \mathrm{P}^{\mathrm{LT}}} + 1$. With N_B non-decreasing bid blocks, the number of distinct bid curves is:

$$|\mathrm{A}_{\mathrm{i}}^{\mathrm{LT}}| = \left(\frac{\mathrm{M}^{\mathrm{LT}} + \mathrm{N}_{\mathrm{B}} - 1}{\mathrm{N}_{\mathrm{B}}} \right) \tag{48}$$

Day-ahead market: spot-market bid prices are discretized at the specified step and combined into non-decreasing three-block curves. The action-space size is:

$$|\mathrm{A}_{\mathrm{i}}^{\mathrm{DA}}| = \left(\frac{\mathrm{M}^{\mathrm{DA}} + \mathrm{N}_{\mathrm{B}} - 1}{\mathrm{N}_{\mathrm{B}}} \right) \tag{49}$$

Every action $a_i = (p_{i,1}, p_{i,2}, \ldots, p_{i,N_B})$ satisfies $p_{i,1} \le p_{i,2} \le \ldots \le p_{i,N_B}$, and each bid block $C_{i,1}, C_{i,2}, \ldots, C_{i,N_B}$ has a predetermined declared quantity (MWh).

Intraday and real-time actions select dispatchable power using updated forecasts and equipment states. Thermal and hydropower participants choose among 50%, 75%, and 100% dispatchable fractions. For thermal units, these fractions apply to increments above minimum technical output. Associated storage has five actions: hold, half-power charging, full-power charging, half-power discharging, and full-power discharging. Frozen day-ahead bid curves remain in use during intraday and real-time operation. Real-time dispatchable ranges depend jointly on intraday schedules and current physical conditions.

(3) Immediate Reward

Generators receive rewards from stage-specific settlement and execution outcomes. Medium- and long-term rewards reflect contracting returns; spot-stage rewards reflect actual delivery, operating costs, and contract-performance feedback.

Medium- and long-term market:

$$\mathrm{r}_{\mathrm{i}}^{\mathrm{LT}} = \sum_{\mathrm{b}=1}^{3} (\mathrm{MCP} \cdot \mathrm{E}_{\mathrm{i,b}}) - \mathrm{C}_{\mathrm{i}}^{\mathrm{thermal/hydro/re}} \left(\sum_{\mathrm{b}} \mathrm{E}_{\mathrm{i,b}} \right) \tag{50}$$

Here, MCP is the medium- and long-term clearing price, E is awarded energy in the corresponding block, and C is its cost function. The reward evaluates participants' contracting decisions at this stage.

Spot stages: day-ahead, intraday, and real-time policies are evaluated from actual execution. Each 15 min reward equals energy-settlement revenue minus operating cost, delivery-shortfall penalties, and incremental K-recovery feedback. Terminal storage-energy deviation is included at cycle-end:

$$r_{i,t}^{exec} = R_{i,t}^{E} - C_{i,t} - F_{i,t}^{short} - \beta_K \Delta K_{i,t} - 1_{t=T} \kappa_E |E_{i,T} - E_{i,T}^{ref}| \tag{51}$$

Here, R^{E} denotes energy-settlement revenue, C denotes operating cost, and $\mathrm{F}^{\mathrm{short}}$ denotes the delivery-shortfall penalty. ΔK is the interval increment in cumulative K-recovery, with $\beta_{\mathrm{k}} = 0.3$. Terminal-energy deviation is measured against the day-ahead terminal target and penalized only at cycle-end, with $\kappa^{\mathrm{E}} = 600$ CNY/MWh. Thermal operating cost includes fuel, fixed online cost, and start-up/shutdown expenses. Renewable-storage cost includes plant fixed expenses and storage charging and discharging costs.

Energy-settlement revenue comprises contract cash flow, the day-ahead difference relative to contracts, and the actual-delivery difference relative to the day-ahead schedule:

$$R_{i,t}^{E} = C_{i,t}^{LT} + (q_{i,t}^{DA} - q_{i,t}^{LT}) \lambda_t^{DA} + (q_{i,t}^{act} - q_{i,t}^{DA}) \lambda_t^{RT} \tag{52}$$

Here, C^{LT} is contract cash flow. Quantities q^{LT}, q^{DA}, and $\mathrm{q}^{\mathrm{act}}$ denote decomposed contract energy, day-ahead awarded energy, and actual delivered energy (MWh), respectively.

Prices λ^{DA} and λ^{RT} are day-ahead and real-time settlement prices. Intraday adjustments enter real-time difference settlement through actual delivery. Day-ahead and intraday rewards aggregate executed rewards over the corresponding hour; real-time rewards use the corresponding 15 min interval. Thermal compensation and full periodic K-recovery are accounted for separately in final financial bills.

$K_{i,t}^{cum}$ is cumulative K-recovery amount:

$$K_{i,t}^{cum} = \begin{cases} k(A_{i,t} - nQ_{i,t})(\overline{p}_t^s - p^c), & \phi_{i,t} > n, \overline{p}_t^s > p^c, \\ k(mQ_{i,t} - A_{i,t})(p^c - \overline{p}_t^s), & \phi_{i,t} < m, p^c > \overline{p}_t^s, \\ 0, & \text{others}, \end{cases} \quad (53)$$

where $A_{i,t}$ and $Q_{i,t}$ are cumulative actual settled energy and cumulative contract energy through interval t, respectively (MWh). $\overline{p}_t^s$ and p^c are the cumulative average real-time price and medium- and long-term contract price, respectively (CNY/MWh). $\phi_{i,t} = A_{i,t}/Q_{i,t}$ is the cumulative contract-performance rate. The lower and upper limits are $m = 0.90$ and $n = 1.10$, and k = 1.05 is the recovery multiplier. $\Delta K_{i,t} = K_{i,t}^{cum} - K_{i,t-1}^{cum}$ is the incremental K-recovery feedback in the current interval. Recovery is not triggered when the performance rate is outside the limits but the price difference is unfavorable.

3.2. WoLF-PHC Multi-Agent Reinforcement-Learning Algorithm

WoLF-PHC is a Q-learning-based multi-agent reinforcement-learning algorithm with policy hill climbing. It maintains a current policy π_i and an average policy $\overline{\pi}_i$, and changes the learning rate according to whether the agent is winning or losing relative to the average policy δ. When the current policy has a higher expected value, the agent uses the smaller learning rate δ_w. Otherwise, it adapts more rapidly using the larger rate δ_l, where $\delta_l \gg \delta_w$.

(1) The WoLF-PHC variables and their initial values are summarized in Table 3.

Table 3. Variable definitions and initial values.

Parameter	Medium- and Long-Term Market	Day-Ahead Market	Intraday Market	Real-Time Market
Training rounds	Monthly: 2000; weekly: 2000	2000	2000	2000
Q-learning rate α	0.1	$\max(0.1 \times 0.997^n, 0.01)$	Same as day-ahead	Same as day-ahead
Discount factor γ	0.9	0.9	0.9	$0.9^{1/4} \approx 0.9740$
Initial win/loss step	0.02/0.04	0.02/0.04	0.02/0.04	0.02/0.04
Minimum win/loss step	0.001/0.002	0.001/0.002	0.001/0.002	0.001/0.002
Policy-decay rate d	0.98	0.995	0.995	0.995
Initial Q-value/policy	0/uniform distribution	0/uniform distribution	0/uniform distribution	0/uniform distribution

Stage-specific policy initialization: medium- and long-term generator learning and spot-market learning maintain separate Q-values, current policies, average policies, and state-visit counts. Consumers learn at the day-ahead submission layer. Spot-market generators maintain separate day-ahead, intraday, and real-time policies, updated at the corresponding decision times within the same training round. Q-values and visit counts start at zero; current and average policies are uniform over feasible actions. In Table 3, n denotes the training round. The 2000 rounds for the three spot stages belong to the same operating-training sequence. Day-ahead and intraday discounting uses 0.9 per hour; the 15 min real-time discount is the fourth root of 0.9.

Operating-boundary initialization: each round loads decomposed contracts, day-ahead load and renewable forecasts, and initial equipment states. Thermal initialization includes output, commitment, and continuous online/offline duration. Hydropower initialization includes output, available water inventory, and volume limits. Storage initialization includes energy, SOC, and power limits. Historical contract performance informs day-ahead states. After the full-day schedule is formed, intraday and real-time operation inherit executed states and revise subsequent schedules as forecasts update. Unit states, water inventory, and storage energy are updated continuously.

Each training round loads medium- and long-term contract inputs, freezes day-ahead bids, and executes intraday rolling adjustment and real-time feedback balancing. At their decision times, participants select bid curves, quantities, or operating actions. Actual delivery generates settlement and operating feedback for Q-value, average-policy, and current-policy updates.

(2) Iterative procedure:

All participants use the same WoLF-PHC update framework with their own stage-specific states, feasible actions, and rewards. Each round follows the steps below until the prescribed training-round limit is reached.

Step 1: Choose the action

During medium- and long-term and day-ahead bidding, generators sample non-decreasing three-block curves from their current state-dependent policies. Consumers select day-ahead load-adjustment ratios. During intraday and real-time operation, generators choose dispatchable power or charging/discharging actions using updated forecasts, actual equipment states, and reference energy. Actual renewable output is revealed after action selection.

Step 2: Environmental interaction and rewards

Day-ahead clearing determines the full-day schedule from frozen bids and equipment constraints. Intraday rolling clearing revises remaining schedules using updated forecasts. Real-time operating actions use ultra-short-term forecasts; current actual output is then revealed for balancing. Actual delivery determines energy revenue, operating costs, and contract-performance feedback for stage-specific policy updates. Intraday changes enter real-time difference settlement through actual delivery. Equipment states, water inventory, and storage energy then advance to the next decision time, completing the state–action–clearing and execution–reward–next-state learning sequence.

Step 3: Updating the Q value

The agent uses its immediate reward r_i and the maximum Q-value of the next state $Q_i(s, a_i)$ to update the Q-value according to the Q-learning rule:

$$Q_i(s, a_i) \leftarrow (1 - \alpha) Q_i(s, a_i) + \alpha \left(r_i + \gamma \max_{a_i'} Q_i(s', a_i') \right) \tag{54}$$

The maximum next-state Q-value estimates returns from subsequent feasible actions. Day-ahead Q-values compare bid curves, whereas intraday and real-time Q-values compare dispatchable-power or charging/discharging actions. They jointly reflect how equipment states, forecast changes, contract performance, and stored energy affect future returns.

Step 4: Update the average strategy

The average policy $\overline{\pi}_i$ represents an agent's historical mean behavior. The visit count for state s $C(s) \leftarrow C(s) + 1$ is updated first, after which the average policy is updated as follows:

$$\overline{\pi}_i(s, a_i) \leftarrow \overline{\pi}_i(s, a_i) + \frac{1}{C(s)} (\pi_i(s, a_i) - \overline{\pi}_i(s, a_i)) \tag{55}$$

The average policy records historical selection probabilities for feasible actions within a state. Day-ahead actions are bid curves; intraday and real-time actions are dispatchable

power or charging/discharging decisions. Current and average policies are compared over the same state and feasible-action set, providing each participant's win/loss benchmark.

Step 5: Judge the win/loss status

Within the same stage and state, each participant calculates expected Q-values under its current and average policies. Their difference determines win/loss status:

$$\Delta = \sum_{a_i} \pi_i(s, a_i) Q_i(s, a_i) - \sum_{a_i} \overline{\pi}_i(s, a_i) Q_i(s, a_i) \tag{56}$$

If $\Delta > 0$, the expected return of the current policy exceeds that of the average policy and the agent is considered to be winning; otherwise, it is considered to be losing. The learning rate is selected accordingly:

$$\delta = \begin{cases} \delta_w, & \Delta > 0 \\ \delta_l, & \Delta \leq 0 \end{cases} \tag{57}$$

Step 6: Update the current strategy

To keep the updated policy as a valid probability distribution, the adjustment bound for each action is calculated as (δ_{sa_i}):

$$\delta_{sa_i} = \min\left(\pi_i(s, a_i), \frac{\delta}{|A_i|-1}\right) \tag{58}$$

The policy hill-climbing step makes small adjustments to the current policy so that it progressively favors the optimal action. First, determine the optimal action in state s, $a^* = arg\max_{a_i} Q_i(s, a_i)$. Then, for each action a_i, calculate the adjustment:

$$\Delta_{sa_i} = \begin{cases} -\delta_{sa_i} & a_i \neq \arg\max_{a'} Q(s, a') \\ \sum_{a' \neq a_i} \delta_{s,a'} & a_i \text{ is optimal} \end{cases} \tag{59}$$

The adjustments in Equation (59) increase selection probabilities for higher-Q actions and adjust the probabilities of other feasible actions accordingly. This update applies separately to day-ahead bid curves and intraday and real-time operating actions. The current policy is then updated as follows:

$$\pi_i(s, a_i) \leftarrow \pi_i(s, a_i) + \Delta_{sa_i} \tag{60}$$

After the update, the policy vector is projected onto the probability simplex so that $\pi_i(s, a_i) \geq 0$ and $\sum_{a_i} \pi_i(s, a_i) = 1$. In practice, negative values are set to zero and the remaining probabilities are renormalized.

Step 7: Convergence Assessment

Repeat Steps 1–6 until the policy change is below a prescribed threshold (e.g., $\max_{a_i} |\pi_i(s, a_i) - \pi_i^{\text{old}}(s, a_i)| < \varepsilon$) or the maximum number of iterations is reached. The complete iterative procedure is summarized in Figure 3.

3.3. AI-Assisted Preparation of Figures 1–3

Figures 1–3 were prepared using an author-directed, AI-assisted workflow. The underlying methodological concepts, market architecture, agent structure, algorithmic workflow, technical relationships, and source materials were developed and provided by the authors. ChatGPT 6.1 sol's image-generation functionality was used to produce preliminary visual drafts based on these author-supplied descriptions and materials. The authors subsequently reviewed and substantially revised the drafts, including their layouts, labels, symbols, connections, and technical relationships, and produced the final figures. ChatGPT was not used to formulate the proposed method, generate or analyze research data, or interpret the

results. The authors verified the final figures and take full responsibility for their accuracy and originality.

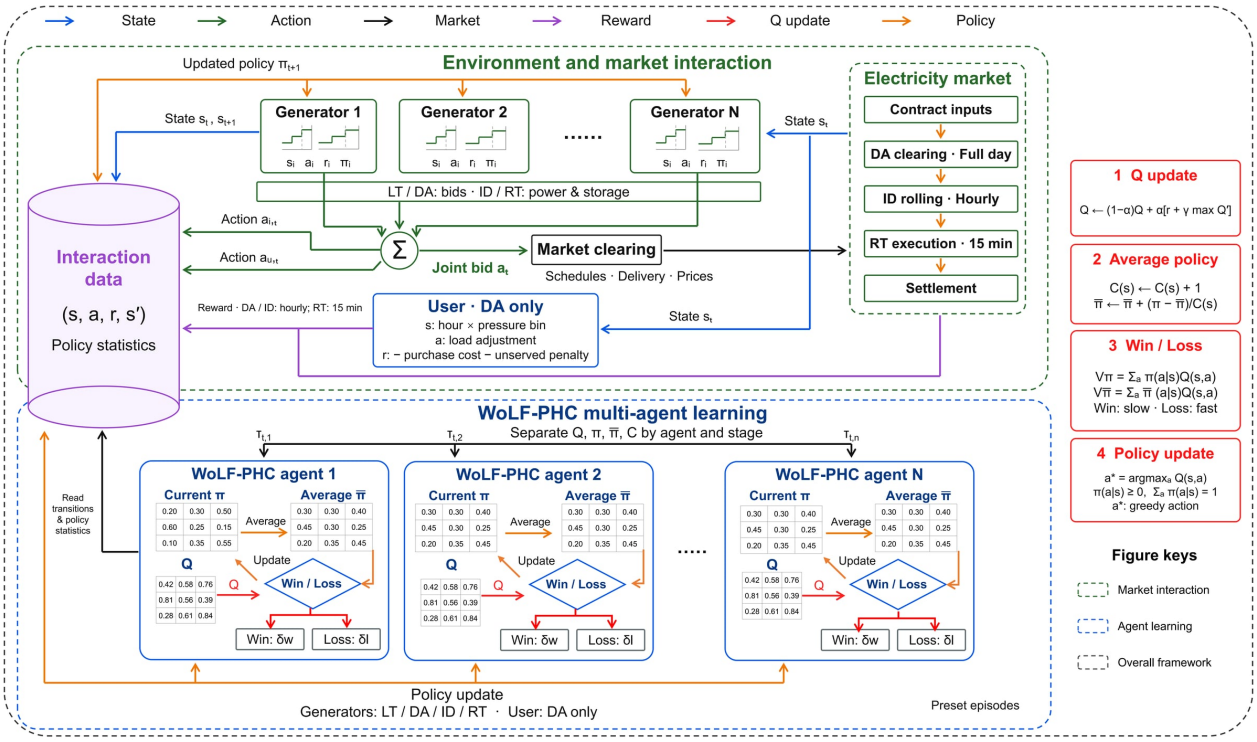


Figure 3. WoLF-PHC solution framework.

4. Results and Discussion

4.1. Case Study

The case study includes three thermal units, one hydropower unit, and two joint renewable-storage participants. renewable1 is a 616-MW wind plant, and renewable2 is a 160-MW photovoltaic plant. Each has 600 MWh of storage, maximum charging and discharging power of 100 MW, charging and discharging efficiencies of 95%, and initial SOC of 50%. The input time series, bid discretization rules, technical and economic parameters, and initial operating conditions are provided in Appendix A. The main asset parameters used in the joint-operation case are summarized in Table 4.

Table 4. Main asset parameters under joint operation.

Participant	Type	Renewable Capacity (MW)	Maximum Output/Delivery (MW)	Storage Energy Capacity (MWh)	Maximum Charging Power (MW)	Maximum Discharging Power (MW)	Initial SOC
thermal1	thermal	—	591	0	0	0	—
thermal2	thermal	—	310	0	0	0	—
thermal3	thermal	—	400	0	0	0	—
hydro1	hydro	—	100	0	0	0	—
renewable1	wind +storage	616	716	600	100	100	50%
renewable2	PV +storage	160	260	600	100	100	50%

Figure 4 shows morning and evening load peaks. Day-ahead forecasts capture the overall trend but underestimate actual demand from midday to evening. renewable1 maintains high output throughout the day, with considerably stronger actual fluctuations than its smooth forecast. renewable2 generates mainly during daylight; actual morning-to-midday output generally exceeds forecasts, followed by pronounced afternoon fluctuations. Renewable variability and its timing relative to peak demand create opportunities for storage to absorb surplus energy, smooth delivery, and shift energy across intervals.

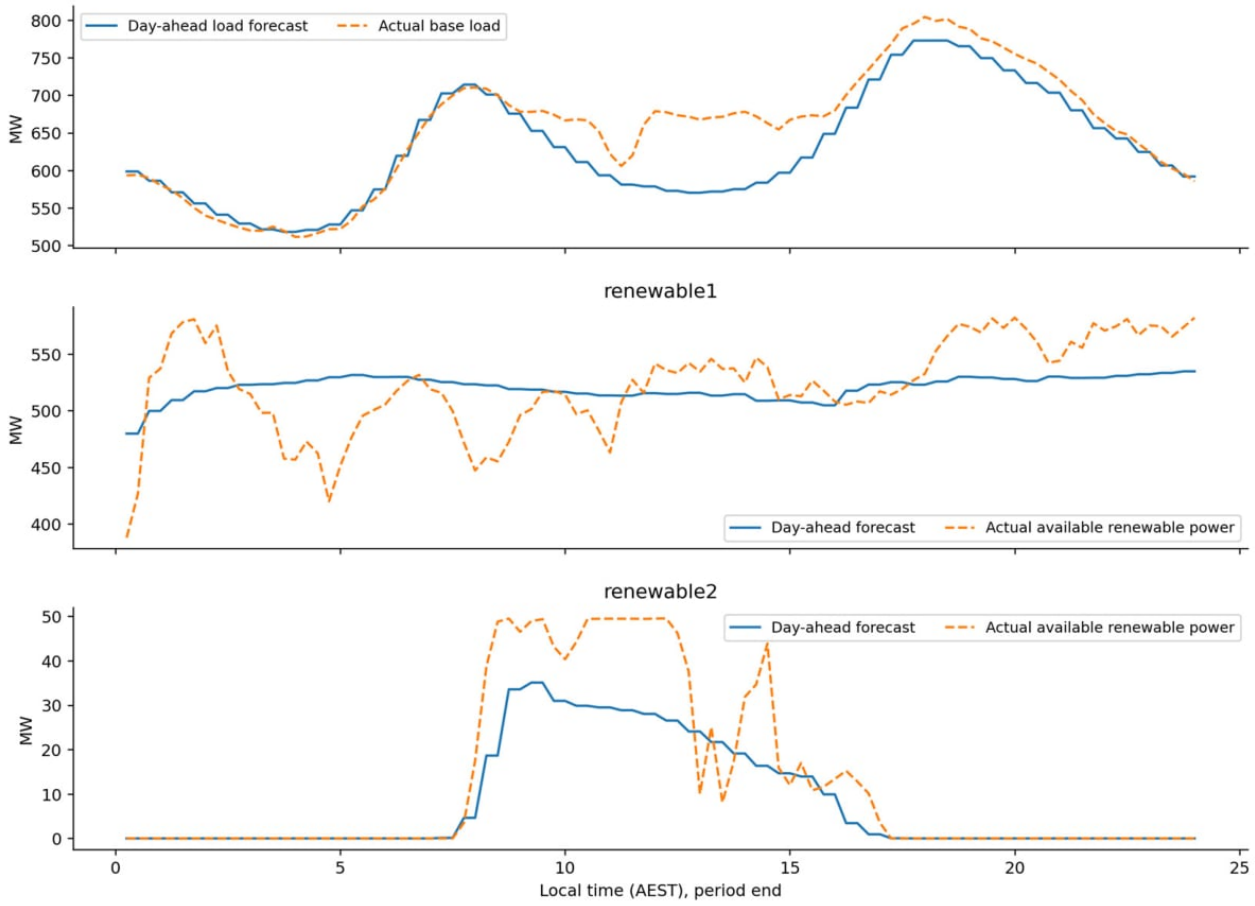


Figure 4. System load and renewable power: forecasts and actual output.

Figure 5 shows total generator-side reward and operating profit during training. Moving averages (MAs) use a 100-round window. Both increase rapidly early in training. Between rounds 1 and 200, the reward MA rises from CNY 2.9457 million to CNY 3.6122 million, and the operating-profit MA rises from CNY 3.1126 million to CNY 3.6820 million. After approximately round 200, the curves fluctuate around a plateau. The operating-profit MA mainly ranges from CNY 3.5624 million to CNY 3.8216 million, ending at CNY 3.7234 million. Training shows rapid early improvement followed by a relatively stable average, while round-to-round fluctuations persist. Training rewards provide learning feedback, whereas final operating profit represents economic returns after full settlement. Subsequent evaluation uses final operating profit as the principal economic indicator. These curves provide context for the following operating and settlement analyses.

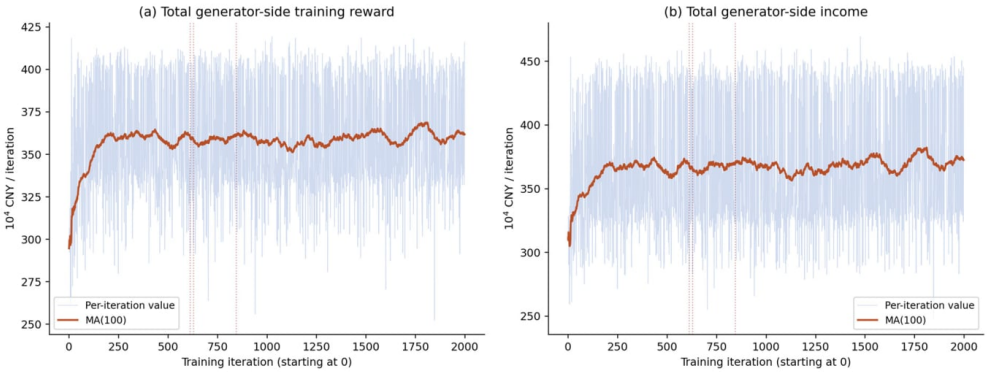


Figure 5. Total generator-side training reward and operating profit.

Table 5 reports final generator-side profit of 372.34 ± 50.26 in CNY 10,000 over the last 100 rounds. The wind-storage and photovoltaic-storage portfolios yield 308.84 ± 30.35 and 3.28 ± 9.91, respectively. Their combined mean profit is CNY 3.1213 million, accounting for most generator-side returns. Round-to-round variability is particularly pronounced relative to the smaller photovoltaic-storage return. Average economic performance and individual-round outcomes should be evaluated separately.

Table 5. Economic indicators over the final 100 joint-operation training rounds (1901–2000).

Indicator (CNY 10,000/Round)	Joint Operation, Mean ± Standard Deviation (SD)
Final generator-side profit	372.34 ± 50.26
Final wind-storage profit	308.84 ± 30.35
Final photovoltaic-storage profit	3.28 ± 9.91
Renewable-storage portfolio profit	312.13 ± 39.32
Final consumer cost	566.49 ± 24.72
Generator operating cost	175.57 ± 30.16
K-recovery	13.67 ± 7.95
Delivery-shortfall penalty	4.91 ± 1.32

The mean and standard deviation describe the average and dispersion of observations, respectively. Confidence intervals express uncertainty in parameter estimation. For a 95% interval procedure, approximately 95% of intervals constructed from repeated samples under identical conditions would cover the true parameter. A two-sided significance test evaluates evidence against the null hypothesis while considering differences in both directions.

When observations may be heteroskedastic and autocorrelated, the Newey–West heteroskedasticity and autocorrelation consistent (HAC) estimator uses lagged residual correlations to estimate regression-coefficient standard errors. These support confidence intervals and significance tests. For multiple hypotheses, Holm's procedure orders raw p-values and adjusts rejection thresholds sequentially to control the probability of at least one false rejection across the family.

Table 5 summarizes rounds 1901–2000, with standard deviations calculated using the window size as denominator. To compare training stages, 2000 rounds are divided into 20 non-overlapping 100-round windows, giving 19 adjacent-window comparisons. Each two-sided test retains the original order of 200 consecutive rounds and regresses profit on an indicator for the later window. The coefficient estimates the later-minus-earlier mean

difference, which is tested against zero. HAC covariance estimation uses Bartlett weights, four lags, and the $n/(n-k)$ correction, where n is sample size and k is the number of regression parameters. Table 6 reports individual normal-approximation 95% intervals, two-sided raw *p*-values, and Holm-adjusted *p*-values for all 19 comparisons.

Table 6. Differences in mean generator-side profit between adjacent 100-round windows (CNY 10,000 per round).

Earlier Window	Later Window	Mean Difference	95% HAC Interval	Raw *p*	Holm *p*
1–100	101–200	22.20	[10.37, 34.04]	0.0002	0.0045
101–200	201–300	−0.59	[−13.16, 11.98]	0.9270	1.0000
201–300	301–400	−0.45	[−13.98, 13.08]	0.9483	1.0000
301–400	401–500	−5.23	[−18.23, 7.77]	0.4302	1.0000
401–500	501–600	8.70	[−6.65, 24.05]	0.2665	1.0000
501–600	601–700	−5.02	[−19.98, 9.94]	0.5106	1.0000
601–700	701–800	0.97	[−12.41, 14.34]	0.8872	1.0000
701–800	801–900	5.43	[−7.26, 18.11]	0.4018	1.0000
801–900	901–1000	−3.98	[−17.98, 10.02]	0.5775	1.0000
901–1000	1001–1100	−6.25	[−21.64, 9.14]	0.4261	1.0000
1001–1100	1101–1200	4.92	[−10.17, 20.01]	0.5230	1.0000
1101–1200	1201–1300	−5.69	[−20.03, 8.66]	0.4372	1.0000
1201–1300	1301–1400	10.68	[−2.96, 24.32]	0.1248	1.0000
1301–1400	1401–1500	−1.51	[−16.05, 13.02]	0.8385	1.0000
1401–1500	1501–1600	−1.66	[−16.46, 13.14]	0.8262	1.0000
1501–1600	1601–1700	−0.36	[−14.38, 13.66]	0.9602	1.0000
1601–1700	1701–1800	12.32	[−2.15, 26.79]	0.0952	1.0000
1701–1800	1801–1900	−15.02	[−28.80, −1.24]	0.0326	0.5872
1801–1900	1901–2000	6.87	[−7.13, 20.88]	0.3363	1.0000

Mean final profit increases from CNY 3.4600 million in rounds 1–100 to CNY 3.6820 million in rounds 101–200. The difference is CNY 222,000, with a 95% interval of CNY [103,700, 340,400] and Holm-adjusted $p = 0.0045$. The mean for rounds 201–300 is CNY 3.6761 million, close to the preceding window. No subsequent adjacent comparison is significant after adjustment. A local decline of CNY 150,200 occurs from rounds 1701–1800 to 1801–1900, with raw $p = 0.0326$ and adjusted $p = 0.5872$. This indicates that the later plateau still contains fluctuations. Together, the curves and window comparisons show rapid improvement over approximately the first 200 rounds, followed by fluctuations around a higher average level.

These tests evaluate profit changes at the 100-round scale along a single training trajectory for this case. Inference assumes some local stability and weak dependence within windows. The absence of significant later adjacent-window differences supports a description of relatively stable average returns in this case. Robustness across random seeds and mean differences between participation modes require separate tests. The following analysis

examines final-round power balance, storage operation, market prices, and settlement to evaluate framework operation.

The upper panel of Figure 6 shows real-time cleared supply by resource. renewable1 is the wind-storage participant. Its larger installed capacity and sustained wind availability make it the main supplier throughout the day. renewable2 is the photovoltaic-storage participant; its smaller capacity, shorter generation window, and low irradiance on the study day limit its cleared energy. Hydropower combines low cost with flexibility, clearing in most intervals and adjusting output with system demand.

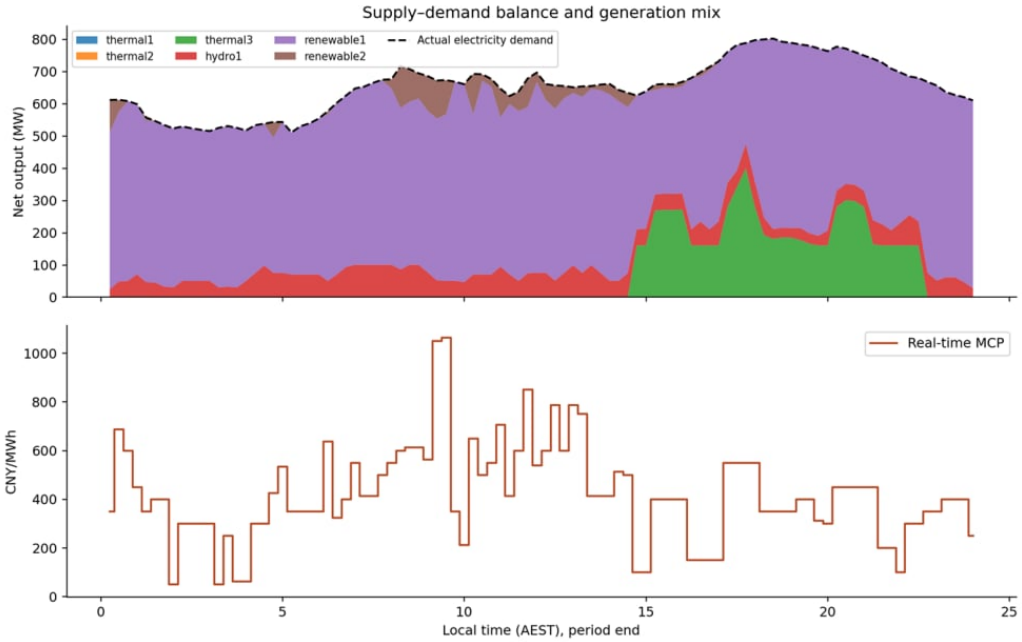


Figure 6. Supply–demand balance and MCP under joint operation.

Thermal supply is mainly provided by thermal3. Its lower start-up cost and 400-MW maximum output favor concentrated afternoon-to-evening operation. It clears from 14:30 to 22:30, operating continuously for eight hours at 160–400 MW. This period covers the evening load peak and declining photovoltaic output, complementing renewable and hydropower supply. Minimum technical output and eight-hour minimum up/down times produce a concentrated output block. Renewable curtailment nevertheless occurs in 19 intervals during thermal operation. Clearing reflects available resources, strategic bids, storage schedules, and thermal commitment constraints jointly.

The lower panel of Figure 6 shows pronounced intraday MCP variation. At 02:00, the price falls to 50 CNY/MWh, reflecting low load and abundant renewable supply; storage absorbs surplus generation. At 09:15–09:30, the MCP rises to 1050–1062.98 CNY/MWh as load increases and renewable supply falls short. Hydropower and storage discharge provide incremental supply at higher marginal cost. At 14:45–15:00, the price falls to 100 CNY/MWh while thermal3 operates at minimum output and storage charges intensively. During the evening peak, the MCP remains at 350 CNY/MWh, with thermal generation and storage jointly supporting supply. These price changes correspond to load, renewable availability, and thermal and storage operating states. Within this case, the framework links changing supply and demand, physical constraints, and price formation while providing trading and adjustment opportunities for joint renewable-storage operation.

Figure 7 shows different storage-use patterns for the two joint participants. Wind-storage inventory falls through the morning and midday, then recovers through afternoon charging. Daily charging and discharging total 429.41 and 357.28 MWh, respectively, with

terminal inventory of 331.86 MWh. Sustained wind availability supplies energy for replenishment, while alternating charging and discharging adjusts delivery across intervals. Photovoltaic-storage charges 56.85 MWh and discharges 196.07 MWh. Inventory falls overall to 147.62 MWh, indicating that some initial stored energy supplements renewable delivery.

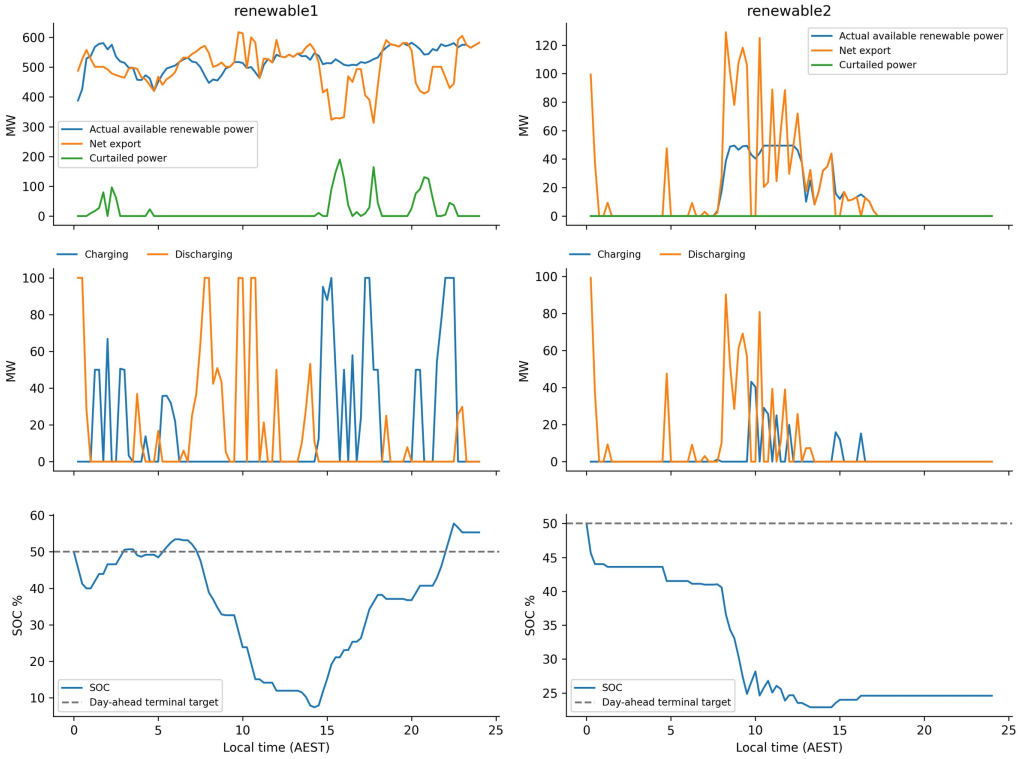


Figure 7. Operating states of renewable1 and renewable2 with joint storage.

These differences reflect renewable-output scale, timing, and market-delivery schedules. renewable1 supplies substantial energy throughout the day, supporting inventory recovery. renewable2 generates mainly during daylight, limiting replenishment opportunities. Joint storage charges only from its associated renewable plant, making photovoltaic inventory recovery particularly dependent on daytime energy allocation. Day-ahead clearing sets terminal SOC to 50%; intraday and real-time stages use soft targets with deviation penalties. Rolling clearing can balance supply requirements, trading schedules, and inventory restoration.

Ordinary curtailment is 440.93 MWh for wind-storage and zero for photovoltaic-storage, reflecting differences in renewable availability, charging headroom, and clearing schedules. Both inventories remain within 0–600 MWh, and charging and discharging remain mutually exclusive. Wind-storage inventory ranges from 44.52 to 346.48 MWh; photovoltaic-storage ranges from 137.38 to 300.00 MWh. Terminal energy is 31.86 MWh above and 152.38 MWh below the day-ahead target, respectively. Inventory changes provide additional context for interpreting daily operating profit.

Figure 8 decomposes final operating profit into contract revenue, day-ahead difference-settlement revenue, and real-time deviation-settlement revenue, less operating costs, K-recovery, and delivery-shortfall penalties, plus thermal cost-gap compensation. Total generator-side final profit is CNY 4.4513 million, including CNY 3.4286 million from wind-storage and CNY 478,700 from hydropower. Wind-storage's larger delivery volume and contributions from contract, day-ahead, and real-time cash flows produce its higher profit. Hydropower earns CNY 610,200 in spot-market cash profit; contract adjustments and K-

recovery reduce final operating profit to CNY 478,700, illustrating how full settlement redistributes returns.

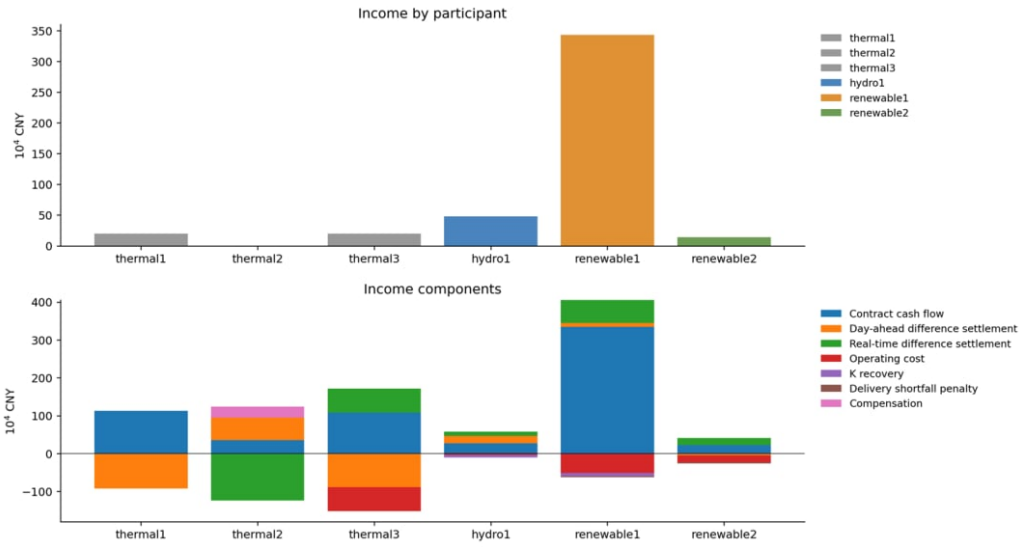


Figure 8. Participant operating profit and its components under joint operation.

Table 7 shows that thermal1 delivers no actual output but earns CNY 201,400 in final profit from historical contract cash flow and day-ahead difference settlement. thermal2 has energy cash flow of CNY −281,600 and receives equal compensation, leaving zero final profit. Photovoltaic-storage final operating profit is CNY 142,500, exceeding its training reward of CNY 51,100. This further distinguishes learning feedback from final financial accounting. Subsequent economic evaluation uses final operating profit, with cash-flow components explaining differences among participants.

Table 7. Three measures of participant returns under joint operation.

Participant	Type	Spot Cash Profit (CNY)	Final Operating Profit (CNY)	Training Reward (CNY)
thermal1	thermal	0	201,448	201,448
thermal2	thermal	0	0	−281,566
thermal3	thermal	6269	199,954	199,954
hydro1	hydro	610,188	478,680	521,707
renewable1	renewable	4,568,118	3,428,639	3,464,185
renewable2	renewable	96,318	142,549	51,118

The K mechanism uses a complete 24 h cycle of 96 intervals, with an allowable performance band of 90–110%. Table 8 shows that recovery is concentrated in hydro1 and renewable1, whose performance rates reach 171.16% and 117.97%, exceeding the upper limit. The cycle-average real-time MCP is 418.99 CNY/MWh, above their mean contract prices of 308.40 and 327.66 CNY/MWh. The resulting favorable differences are 110.59 and 91.32 CNY/MWh. Applying recovery to energy above the tolerance limit gives charges of CNY 61,500 and CNY 78,100. The combined CNY 139,600 is split approximately 44.0% and 56.0%. The mechanism adjusts returns when excess delivery coincides with a favorable real-time price difference.

Table 8. Verification of the periodic K-recovery mechanism.

Participant	Contract Energy (MWh)	Actual Energy (MWh)	Performance Rate	Trigger	Favorable Price Difference	K Charge (CNY)
thermal1	3196.90	0.00	0.00%	None	0.00	0.00
thermal2	1020.91	0.00	0.00%	None	0.00	0.00
thermal3	3073.71	1716.82	55.85%	None	0.00	0.00
hydro1	865.46	1481.36	171.16%	Upper limit	110.59	61,466.78
renewable1	10,214.33	12,050.12	117.97%	Upper limit	91.32	78,090.04
renewable2	658.19	440.01	66.85%	None	0.00	0.00

Performance rates for thermal1, thermal2, thermal3, and renewable2 are 0%, 0%, 55.85%, and 66.85%, all below 90%. Because the cycle-average real-time price exceeds their contract prices, the current lower-bound rule produces no K charge. Recovery depends jointly on performance deviation and price-difference direction. thermal1 retains CNY 201,400 in contract-to-day-ahead gains, illustrating the boundary of a mechanism assessed against the average real-time price. Overall, when spot prices are below contract prices, the mechanism recovers favorable gains from contract underperformance and constrains strategic deviation from contracted schedules.

The correspondence among power balance, price variation, resource adjustment, and settlement supports the operational consistency of the proposed framework in this case. It also illustrates the contribution of joint renewable-storage operation to energy delivery and flexibility.

4.2. Economic Value and Renewable Utilization Under Two Operating Scenarios

Table 9 compares joint operation and independent participation using operating results for 2 June 2026, with identical load, renewable inputs, and medium- and long-term contract accounting. Under joint operation, each renewable resource and its associated storage submit bids as one participant, and storage charges from that renewable resource. Under independent participation, renewable generation and storage bid separately, and storage may purchase electricity from the market. The two scenarios have identical total storage capacity, power ratings, efficiencies, and initial SOC. Renewable returns aggregate each renewable asset and its associated storage, using consistent income, energy, and cost accounting across the two scenarios.

To ensure comparability, returns, net energy sold, and per-kWh electricity costs use a consistent storage-inventory valuation basis. Returns account for operating costs, K-recovery, and delivery-shortfall penalties. Curtailment and delivery shortfalls use actual operating results, while consumer procurement costs use actual settlement bills.

Figure 9 compares generator-side returns, spot-market cash profit, and training rewards. Joint-operation generator-side returns are CNY 3.7296 million, exceeding independent participation at CNY 3.4177 million by CNY 311,900. Independent participation yields higher spot-market cash profit, at CNY 3.8092 million, compared with CNY 3.6588 million under joint operation. The different rankings show that economic value depends jointly on spot trading, medium- and long-term and day-ahead difference settlement, contract-performance charges, and operating costs. The complete return measure captures their combined effects.

Table 9. Settings and key differences between the two scenarios.

Scenario	Bidding Arrangement	Storage Assets
Joint operation	Renewable generation and storage bid jointly; storage charges from the associated renewable plant	600 MWh/100 MW each for wind-storage and photovoltaic-storage
Independent participation	Renewable generation and storage bid separately; market purchases are permitted	600 MWh/100 MW for each associated storage system

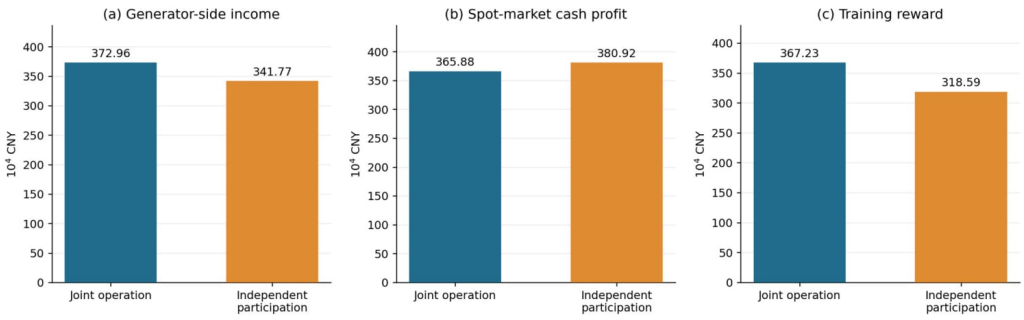


Figure 9. Generator-side income, spot-market cash profit and training reward across two scenarios.

Training rewards are CNY 3.6723 million and CNY 3.1859 million for the two scenarios, respectively, representing the learning signals used by the algorithm. Figure 9 uses saved training-reward records directly. Returns and spot-market cash profits use consistent operating-cost accounting, including photovoltaic fixed operating expenses of CNY 31,000/day. Joint operation achieves both a higher learning reward and higher settlement returns. Consumer bills, resource operation, and the portfolio returns below further explain its economic value.

Figure 10 shows consumer procurement costs in the spot market of CNY 5.3724 million under joint operation and CNY 5.6868 million under independent participation. After contract-difference settlement and compensation surcharges, total settlement costs are CNY 5.5736 million and CNY 5.6002 million, respectively. The reported difference is CNY 26,700. In this case, joint operation reduces consumer costs and increases supply-side returns.

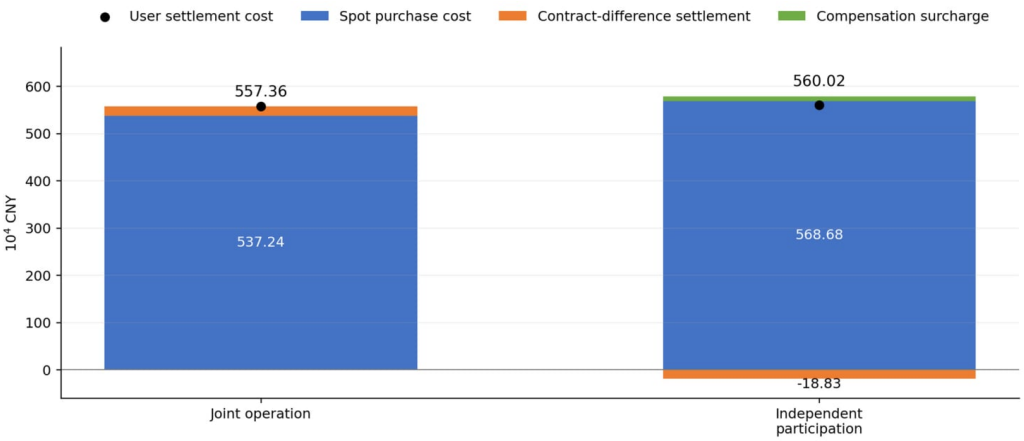


Figure 10. User electricity cost components across two scenarios.

Table 10 shows that joint operation combines higher supply-side returns with lower consumer costs in this case. Generator-side returns reach CNY 3.7296 million, while operating costs are CNY 1.7136 million, CNY 164,100 below independent participation. Higher returns coincide with lower operating expenditure. Consumer settlement costs are similar between the scenarios, while joint operation further increases supply-side returns. Storage value is reflected in both generator returns and consumer payments.

Table 10. Core system indicators for the two scenarios.

Indicator	Joint Operation	Independent Participation
Generator-side returns (CNY 10,000)	372.96	341.77
Spot-market cash profit (CNY 10,000)	365.88	380.92
Training reward (CNY 10,000)	367.23	318.59
Mean MCP (CNY/MWh)	334.77	357.61
Consumer spot cost (CNY 10,000)	537.24	568.68
Consumer settlement cost (CNY 10,000)	557.36	560.02
Delivery shortfall (MWh)	208.35	157.15
Total K-recovery (CNY 10,000)	10.98	2.32
Generator operating cost (CNY 10,000)	171.36	187.77
Delivery-shortfall penalty (CNY 10,000)	4.17	3.14
Renewable utilization (%)	89.00	80.42
Aggregate renewable electricity cost (CNY/kWh)	0.3282	0.3306

Aggregate renewable electricity costs further illustrate this coordination. They are 0.3282 and 0.3306 CNY/kWh under joint operation and independent participation, respectively, a reported reduction of approximately 0.72%. Compared with independent participation, aggregate returns under joint bidding rise from CNY 2.7434 million to CNY 3.0860 million, an increase of approximately 12.49%. Net energy sold rises from 10,272.35 to 11,415.67 MWh, an increase of approximately 11.13%. In this case, joint operation combines higher portfolio returns and net energy sales with lower payments per unit of renewable electricity. Joint operation also incurs CNY 109,800 in K-recovery and CNY 41,700 in delivery-shortfall penalties. Its return advantage includes these contract-performance expenses. The following analysis examines renewable utilization and delivery as the operating basis for these economic outcomes.

Figure 11 explains these economic outcomes through net energy sold, curtailment, and delivery shortfalls for wind and photovoltaic generation. Total curtailment is 1414.41 MWh under joint operation and 2519.01 MWh under independent participation, a reduction of 1104.60 MWh. Renewable utilization rates are 89.00% and 80.42%, respectively. Most of the renewable-integration benefit comes from wind. Joint wind-storage curtailment is 1414.41 MWh, 1101.41 MWh below independent participation, while net energy sold

reaches 11,125.57 MWh. Photovoltaic curtailment is 0 and 3.19 MWh in the two scenarios, with utilization rates of 100.00% and 98.94%, respectively.

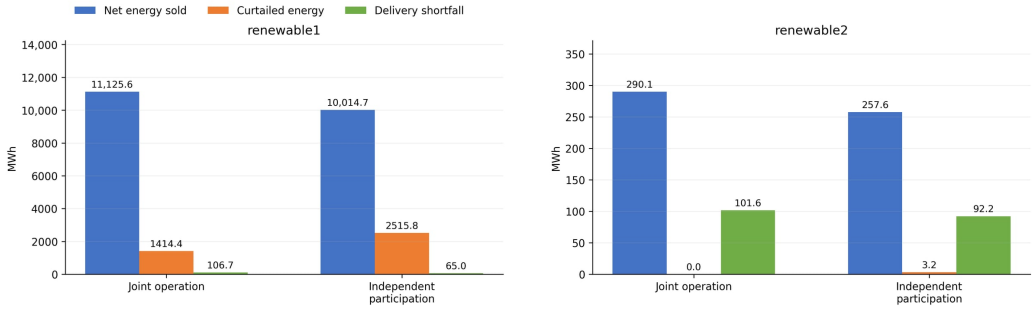


Figure 11. Net energy sold, curtailed energy and delivery shortfall across two scenarios.

Delivery shortfalls show a different pattern. Under joint operation, wind and photovoltaic shortfalls are 106.73 and 101.62 MWh, totaling 208.35 MWh, above the 157.15 MWh under independent participation. Curtailment measures use of available resources, whereas delivery shortfalls measure performance against scheduled delivery; they are subject to different constraints. Joint bidding increases renewable utilization and delivery while incurring the corresponding shortfall penalties, which are included in returns.

Figure 12 aggregates comparable returns for each renewable resource and its associated storage. Wind-side returns are CNY 3.0129 million under joint operation and CNY 2.6731 million under independent participation. Photovoltaic-side returns are CNY 73,100 and CNY 70,300, respectively. Combined portfolio returns are CNY 3.0860 million and CNY 2.7434 million. Joint operation increases total returns by CNY 342,600, of which CNY 339,800 comes from wind. Most of the renewable return improvement arises from wind-storage coordination, with a smaller photovoltaic-storage gain.

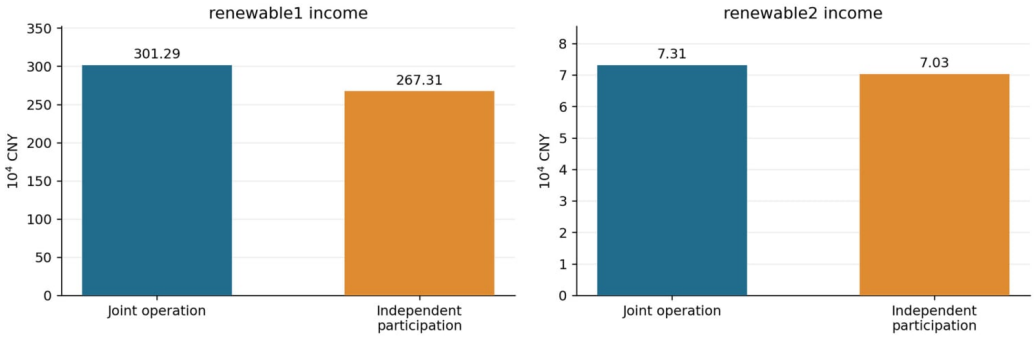


Figure 12. Comparable renewable–storage portfolio income across two scenarios.

Table 11 shows that wind has a larger energy base. Joint operation yields higher net energy sales, lower wind curtailment, and higher returns than independent participation, indicating that joint bidding and internal energy coordination convert more available wind generation into market value. Photovoltaic returns differ less. Joint operation already utilizes all photovoltaic output that day, while independent participation curtails only 3.19 MWh, limiting further energy gains from utilization improvement. Operating expenses, contract adjustments, and performance charges also affect the conversion of revenue into returns. Wind-storage and photovoltaic-storage gains depend on resource scale, output profiles, and settlement conditions.

Table 11. Renewable-storage portfolio returns and operating quantities.

Portfolio	Scenario	Returns (CNY 10,000)	Spot Cash Profit (CNY 10,000)	Curtailment (MWh)	Net Energy Sold (MWh)	Delivery Shortfall (MWh)	Curtailment Rate
Wind	Joint operation	301.29	315.11	1414.41	11,125.57	106.73	11.26%
Wind	Independent participation	267.31	316.14	2515.82	10,014.73	64.96	20.03%
Photovoltaic	Joint operation	7.31	1.63	0.00	290.10	101.62	0.00%
Photovoltaic	Independent participation	7.03	7.84	3.19	257.62	92.20	1.06%

Overall, joint operation provides both economic and renewable-integration value in this case. Generator-side and aggregate renewable returns are higher under joint operation, with wind-storage contributing most of the gain and photovoltaic-storage also improving slightly. Joint operation further reduces wind and photovoltaic curtailment, raises renewable utilization, and converts available resources into useful supply. These results reflect the combined operating value of joint bidding, resource adjustment, and settlement mechanisms within the proposed framework.

4.3. Joint Renewable-Storage Operation at Different Storage Capacities

The preceding two-scenario comparison examines economic and renewable-integration value. To further evaluate the joint electricity energy market simulation framework, this section varies storage energy capacity under joint operation. Operating results from 2 to 4 June 2026, covering 288 consecutive intervals, are used to analyze how wind-plant profit changes with associated storage capacity. All indicators use the same three-day cumulative basis, linking operating trajectories with settlement results.

All configurations use identical three-day load and renewable inputs. Wind-storage power remains at 100 MW. Initial SOC is 50%, and inventory carries continuously across days. K-recovery and delivery-shortfall penalties follow the prescribed rules.

Figure 13 shows higher morning and evening demand and lower early-morning and midday demand across the three days. Wind supplies energy throughout the day, although actual output falls substantially below forecasts on the afternoon of 4 June. Three-day wind energy totals 38,900 MWh, providing the operating context for comparing storage capacities.

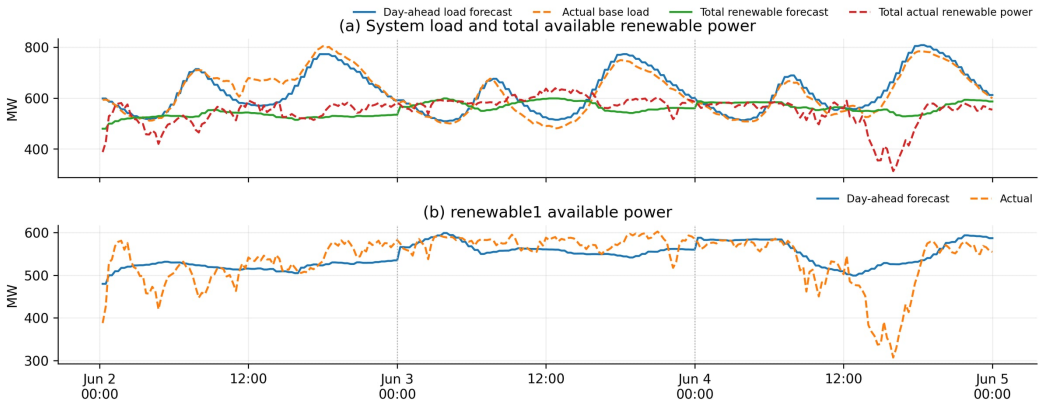


Figure 13. Three-day system load and available renewable power: forecasts and actual output.

The configurations in Table 12 share a no-storage baseline. Wind-storage energy capacities are 200, 400, and 600 MWh, corresponding to storage durations of 2, 4, and 6 h, respectively. Charging and discharging power, efficiency, and plant delivery limits remain unchanged across configurations, allowing operating outcomes to be compared as energy capacity varies at fixed power.

Table 12. Storage-capacity analysis configurations.

Configuration	Power (MW)	Capacity (MWh)	Rated Duration (h)
No-storage baseline	0	0	—
Wind-storage 200	100	200	2
Wind-storage 400	100	400	4
Wind-storage 600	100	600	6

Table 13 shows wind-storage profit increasing from CNY 9.1861 million without storage to CNY 9.9598 million at 200 MWh. It then decreases to CNY 9.6970 million and CNY 9.6765 million at 400 and 600 MWh, respectively. Utilization nevertheless rises from 75.80% to 86.55%, 86.97%, and 87.70%. This round shows continued utilization improvement alongside declining profit as capacity expands beyond 200 MWh.

Table 13. Three-day renewable profit and utilization.

Resource	Capacity (MWh)	Profit (CNY 10,000)	Curtailment (MWh)	Utilization (%)
Wind	0	918.61	9406.40	75.80
Wind	200	995.98	5226.39	86.55
Wind	400	969.70	5066.13	86.97
Wind	600	967.65	4780.61	87.70

In Figure 14, wind-plant profit increases with initial storage deployment but falls as capacity expands further. Renewable utilization continues to rise. Larger capacity improves renewable use in this round, while the extent to which additional trading revenue covers additional costs changes. Together, these responses illustrate the economic and renewable-integration effects of storage capacity.

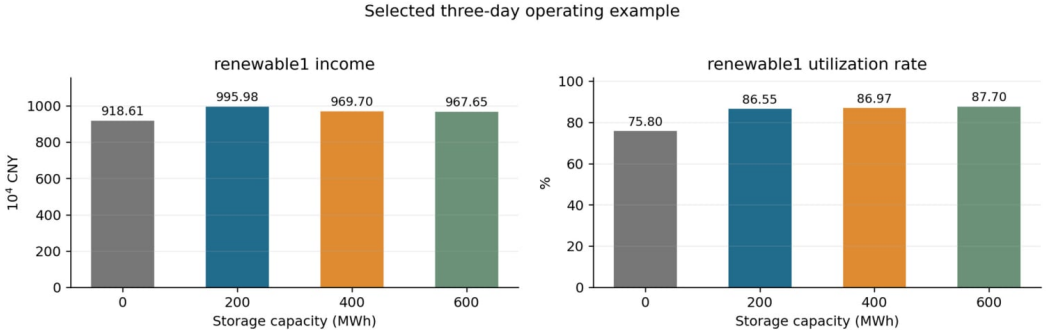


Figure 14. Three-day income and renewable utilization rate at different storage capacities.

Table 14 shows energy-settlement revenue of CNY 11.7227 million at 200 MWh, compared with CNY 11.6075 million and CNY 11.7078 million at 400 and 600 MWh. Expanding from 400 to 600 MWh adds approximately CNY 100,300 in settlement revenue, but allo-

cated construction cost rises by approximately CNY 131,000. Changes in operating and delivery expenses offset part of the additional expenditure, leaving a small profit decline. Storage expansion that improves wind utilization must also cover additional investment and contract-performance expenses.

Table 14. Three-day profit components (CNY 10,000; capacity in MWh).

Resource	Capacity	Energy-Settlement Revenue	Operating Cost	K-Recovery	Delivery Penalty	Allocated Construction Cost	Profit
Wind	0	1058.26	131.64	0.00	8.01	0.00	918.61
Wind	200	1172.27	153.45	0.00	6.30	16.53	995.98
Wind	400	1160.75	153.83	0.00	7.59	29.63	969.70
Wind	600	1170.78	153.80	0.00	6.60	42.72	967.65

Additional capacity that promotes renewable utilization must also cover the associated investment and contract-performance expenses.

Figure 15 and Table 15 show total charging-plus-discharging energy of 715.11, 1333.02, and 1278.63 MWh for 200, 400, and 600 MWh of wind storage, respectively. Throughput changes non-monotonically with capacity. It increases markedly between 200 and 400 MWh but decreases at 600 MWh. Additional capacity use also depends on charging sources, power limits, and trading schedules. Equivalent cycles are 1.79, 1.67, and 1.07, indicating declining utilization per unit of capacity. Larger capacity provides more energy-shifting headroom, but its realized use must be evaluated alongside additional investment and profit.

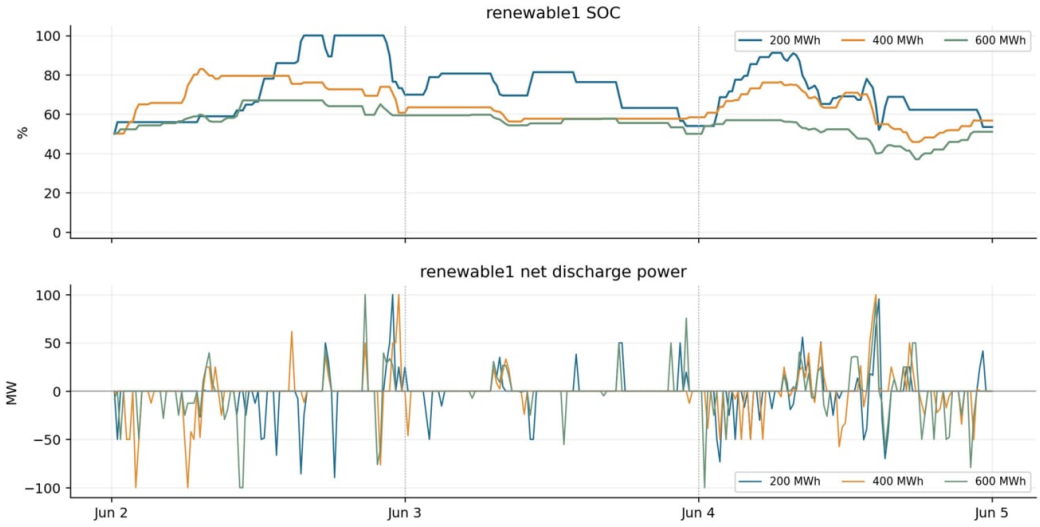


Figure 15. Three-day storage SOC and net charging/discharging power.

Tables 13–15 show renewable profit first increasing and then decreasing with storage capacity, while utilization rises continuously. Moderate storage deployment increases renewable use and trading revenue. Further expansion does not translate proportionally into dispatched energy, weakening revenue coverage of additional costs and reducing profit. Storage expansion should be evaluated jointly against utilization gains and investment returns. The simulated response is consistent with this operating trade-off. Under specified renewable resources and market rules, the framework links charging and discharging with cost and revenue components to analyze joint-operation profit across capacities. It provides a method for evaluating renewable-plant bidding in electricity markets.

Table 15. Three-day storage charging, discharging, and inventory use.

Resource	Capacity (MWh)	Charging (MWh)	Discharging (MWh)	Initial Energy (MWh)	Terminal Energy (MWh)	Equivalent Cycles
Wind	0	0.00	0.00	0.00	0.00	0.00
Wind	200	375.88	339.23	100.00	100.00	1.79
Wind	400	749.96	583.06	200.00	298.71	1.67
Wind	600	722.96	555.67	300.00	401.90	1.07

5. Conclusions

This study develops a multi-participant electricity energy market simulation framework linking medium- and long-term trading, day-ahead clearing, intraday rolling adjustment, and real-time execution. Joint renewable-storage operation, equipment constraints, difference settlement, and contract-performance assessment are integrated within one analysis. WoLF-PHC represents dynamic adjustment of stage-specific bidding and operating actions. Typical-day analysis and comparisons between two renewable participation modes support the following conclusions.

(1) The framework links market prices, resource operation, and settlement to explain bidding and operating outcomes across market time scales. In this case, real-time price changes correspond to load, renewable supply, and conventional-generation and storage adjustment. Clearing satisfies supply-demand balance, storage SOC limits, and mutually exclusive charging and discharging. Participant returns and periodic K-recovery can be recalculated from the settlement rules. These case-study results support the framework's operational rationale and settlement consistency.

(2) In this case, joint renewable-storage operation combines higher supply-side returns with lower consumer costs. Under consistent storage-inventory valuation, renewable returns are CNY 3.0860 million and CNY 2.7434 million for joint operation and independent participation, respectively. Wind-storage provides most of the joint-operation gain, with a smaller photovoltaic-storage improvement. Consumer settlement costs under joint operation are below those under independent participation. Aggregate renewable electricity costs are 0.3282 and 0.3306 CNY/kWh, respectively. Joint operation also reduces wind and photovoltaic curtailment. Coordinated bidding promotes internal energy coordination and converts available renewable resources into useful supply, combining economic and renewable-integration value. Simulations at three storage capacities additionally show that the framework can analyze participant market returns across storage sizes, supporting its effectiveness for this purpose.

This study adopts the basic Pool centralized clearing framework without transmission constraints. Future research will extend the electric energy market simulation framework and establish a joint simulation analysis framework for the electric energy market and ancillary service market to further investigate the coordination among resource allocation, market incentives and operational decisions in electricity markets.

Author Contributions: Conceptualization, Z.C.; methodology, Z.C., X.L., X.G. and Y.G.; investigation, Z.C., X.L., X.G., Y.G., Y.Z. and Y.S.; formal analysis, Y.Z. and Y.S.; writing—original draft preparation, Z.C., X.L. and Y.G. All authors have read and agreed to the published version of the manuscript.

Funding: This research is supported by the Science and Technology Project of State Grid Jibei Electric Power Company Limited (Grant No. B3018K25Z013).

Data Availability Statement: The original contributions presented in the study are included in the article, further inquiries can be directed to the corresponding author.

Acknowledgments: During the preparation of Figures 1–3, the authors used ChatGPT 6.1 sol (OpenAI; image-generation functionality, accessed in 2026) to generate preliminary visual drafts based on author-developed methodological workflows and source materials. The authors reviewed, substantially revised, and finalized the output and take full responsibility for the content of this publication.

Conflicts of Interest: Authors Zhengpai Cui, Xiaoxue Liu, and Xue Gong were employed by State Grid Jibei Electric Power Company Limited. Authors Yu Gong, Yang Zhao, and Yinchi Shao were employed by State Grid Jibei Electric Power Co., Ltd., Electric Power Science Research Institute. The authors declare that the research was conducted in the absence of any commercial or financial relationships that could be construed as a potential conflict of interest. The authors declare that this study received funding from the Science and Technology Program of State Grid Jibei Electric Power Company Limited. The funder was not involved in the study design, collection, analysis, or interpretation of data, the writing of this article, or the decision to submit it for publication.

Appendix A. Case-Study Data and Model Settings

This appendix provides wind, photovoltaic, and load time series, bid discretization rules, unit and storage parameters, and initial operating conditions.

Appendix A.1. Wind, Photovoltaic, and Load Time Series

Time series are drawn from the New South Wales region (NSW1) of the Australian Energy Market Operator (AEMO) National Electricity Market for 2–4 June 2026. Times use Australian Eastern Standard Time (AEST, UTC+10), and power is reported in MW. Load forecasts use PredispatchIS TOTALDEMAND, while actual load uses historical DISPATCHREGIONSUM.TOTALDEMAND; both are scaled by 2377/31,801. Wind forecasts for RYEPARK1 and photovoltaic forecasts for DARLSF1 use UIGF, while actual generation uses historical SCADA output. Their capacity factors are mapped to 616 MW and 160 MW, respectively.

For operating day D, day-ahead inputs use forecasts for D published on $D-1$. Intraday and real-time inputs use forecasts available at each decision time on D. AEMO time series are aligned and converted to the decision and clearing intervals used in this study. Forecast error equals actual output minus the forecast used for the same target interval.

Table A1. (**a**) Day-ahead wind, photovoltaic, and load forecasts. (**b**) Intraday wind, photovoltaic, and load forecasts. (**c**) Real-time wind, photovoltaic, and load forecasts and actual values.

(**a**)			
Target hour (AEST)	Wind forecast (MW)	PV forecast (MW)	Load forecast (MW)
2 June 2026			
00:00–01:00	489.797000	0.000000	592.379106
01:00–02:00	513.260344	0.000000	563.394819
02:00–03:00	521.461646	0.000000	535.068298
03:00–04:00	523.965750	0.000000	519.772261
04:00–05:00	528.166260	0.000000	524.305611
05:00–06:00	530.650312	0.000000	560.742829
06:00–07:00	528.632271	0.000000	643.314073
07:00–08:00	524.330698	2.370618	708.407441
08:00–09:00	520.730146	26.104727	688.289908

Table A1. *Cont.*

(**a**)			
Target hour (AEST)	Wind forecast (MW)	PV forecast (MW)	Load forecast (MW)
2 June 2026			
09:00–10:00	517.660573	33.021091	641.840454
10:00–11:00	514.331125	29.674182	602.265396
11:00–12:00	514.409729	28.438400	579.871097
12:00–13:00	515.321698	25.304727	571.492436
13:00–14:00	513.978208	20.406109	573.390239
14:00–15:00	508.973208	15.503709	590.258933
15:00–16:00	506.014323	11.920873	632.910166
16:00–17:00	520.387656	2.178909	702.287606
17:00–18:00	524.094885	0.017164	763.494553
18:00–19:00	527.894354	0.000000	769.208143
19:00–20:00	528.697240	0.000000	741.433995
20:00–21:00	528.195135	0.000000	709.961412
21:00–22:00	529.042135	0.000000	668.151446
22:00–23:00	531.490094	0.000000	633.548498
23:00–24:00	534.086438	0.000000	599.198564
3 June 2026			
00:00–01:00	565.659646	0.000000	585.118272
01:00–02:00	574.796979	0.000000	554.807990
02:00–03:00	586.797750	0.000000	526.929572
03:00–04:00	596.058604	0.000000	511.216825
04:00–05:00	591.038365	0.000000	514.868919
05:00–06:00	573.124635	0.000000	547.327776
06:00–07:00	554.485823	0.000000	618.622080
07:00–08:00	553.745500	0.879127	672.289763
08:00–09:00	557.459146	11.650327	648.987300
09:00–10:00	561.642010	20.610327	600.770848
10:00–11:00	561.932365	27.760000	559.650415
11:00–12:00	560.968260	34.943127	532.292977
12:00–13:00	560.065917	38.808436	516.190429
13:00–14:00	555.286302	39.413818	521.700336
14:00–15:00	550.663094	38.354909	550.827014
15:00–16:00	549.362115	34.508800	613.555417
16:00–17:00	549.496062	6.873891	691.414668
17:00–18:00	547.239000	0.015418	756.889989
18:00–19:00	542.744125	0.000000	770.361849
19:00–20:00	547.383375	0.000000	747.630072
20:00–21:00	555.070542	0.000000	720.229655
21:00–22:00	560.011375	0.000000	678.201804
22:00–23:00	561.418229	0.000000	641.155406
23:00–24:00	560.151740	0.000000	607.129870
4 June 2026			
00:00–01:00	585.184760	0.000000	580.127476
01:00–02:00	583.022344	0.000000	553.948036
02:00–03:00	581.505604	0.000000	528.640510
03:00–04:00	582.531469	0.000000	515.351031
04:00–05:00	583.830042	0.000000	519.966227
05:00–06:00	583.512417	0.000000	555.110338
06:00–07:00	583.833250	0.000000	632.111504
07:00–08:00	568.725208	0.899200	686.319975
08:00–09:00	548.823115	14.115200	655.914766

Table A1. *Cont.*

(**a**)			
Target hour (AEST)	Wind forecast (MW)	PV forecast (MW)	Load forecast (MW)
4 June 2026			
09:00–10:00	528.098885	27.900509	605.817703
10:00–11:00	516.261740	41.540945	570.162703
11:00–12:00	510.723354	53.516509	558.444013
12:00–13:00	500.724583	52.089600	558.168574
13:00–14:00	506.886187	42.541382	567.119416
14:00–15:00	519.266344	31.365236	593.503287
15:00–16:00	527.252688	22.932655	645.913741
16:00–17:00	526.569312	4.024727	720.931894
17:00–18:00	530.439365	0.013673	791.821447
18:00–19:00	537.694208	0.000000	805.785883
19:00–20:00	555.449125	0.000000	784.370385
20:00–21:00	576.815823	0.000000	755.422350
21:00–22:00	589.930688	0.000000	707.383046
22:00–23:00	591.937500	0.000000	660.722808
23:00–24:00	588.478115	0.000000	620.395430
(**b**)			
Target hour (AEST)	Wind forecast (MW)	PV forecast (MW)	Load forecast (MW)
2 June 2026			
00:00–01:00	353.692281	0.000000	592.379106
01:00–02:00	479.509479	0.000000	557.070554
02:00–03:00	570.115219	0.000000	533.858907
03:00–04:00	541.585115	0.000000	514.206668
04:00–05:00	512.963573	0.000000	529.627532
05:00–06:00	498.136260	0.000000	553.372118
06:00–07:00	519.208594	0.000000	637.129582
07:00–08:00	578.018146	3.185745	696.584107
08:00–09:00	547.237396	56.689745	670.574714
09:00–10:00	484.305938	89.270982	651.090654
10:00–11:00	523.143615	81.684655	638.432780
11:00–12:00	521.868302	88.071564	627.369239
12:00–13:00	549.269875	73.835927	597.174814
13:00–14:00	539.514938	48.868655	632.019193
14:00–15:00	539.388208	24.898327	666.766775
15:00–16:00	523.826188	19.279127	689.430907
16:00–17:00	518.861292	1.289309	739.317560
17:00–18:00	517.853875	0.005818	790.025299
18:00–19:00	562.799417	0.000000	798.704814
19:00–20:00	554.091198	0.000000	768.829928
20:00–21:00	578.140865	0.000000	735.564186
21:00–22:00	576.369062	0.000000	690.511362
22:00–23:00	564.143708	0.000000	648.611327
23:00–24:00	581.967604	0.000000	610.727773
3 June 2026			
00:00–01:00	590.182542	0.000000	585.118272
01:00–02:00	585.591417	0.000000	554.560954
02:00–03:00	573.605885	0.000000	523.401183
03:00–04:00	566.460927	0.000000	511.447791

Table A1. *Cont.*

(**b**)			
Target hour (AEST)	Wind forecast (MW)	PV forecast (MW)	Load forecast (MW)
3 June 2026			
04:00–05:00	592.895188	0.000000	512.781634
05:00–06:00	582.618094	0.000000	538.687504
06:00–07:00	574.873979	0.000000	612.942873
07:00–08:00	587.642344	1.679127	666.503295
08:00–09:00	575.855729	28.447127	638.967214
09:00–10:00	543.410656	29.888582	564.862459
10:00–11:00	554.133708	36.856727	509.381809
11:00–12:00	543.145167	43.009455	485.562103
12:00–13:00	537.309208	57.400727	484.356449
13:00–14:00	549.308375	59.403055	484.775400
14:00–15:00	549.995760	76.423564	521.392756
15:00–16:00	581.611479	61.501091	586.864714
16:00–17:00	574.809812	10.773527	665.352953
17:00–18:00	559.457937	0.004945	740.612910
18:00–19:00	578.956583	0.000000	745.590251
19:00–20:00	591.427375	0.000000	723.952009
20:00–21:00	605.981979	0.000000	691.455405
21:00–22:00	603.044750	0.000000	658.133230
22:00–23:00	592.134812	0.000000	628.676548
23:00–24:00	557.133500	0.000000	596.487524
4 June 2026			
00:00–01:00	603.869292	0.000000	580.127476
01:00–02:00	580.879979	0.000000	547.848383
02:00–03:00	583.723365	0.000000	519.889986
03:00–04:00	581.593031	0.000000	512.986439
04:00–05:00	568.451698	0.000000	523.296165
05:00–06:00	567.947990	0.000000	544.053524
06:00–07:00	549.700594	0.000000	615.635974
07:00–08:00	560.932969	1.005673	668.908251
08:00–09:00	545.463990	13.774836	650.629097
09:00–10:00	506.620698	19.043491	580.922401
10:00–11:00	505.765677	45.691345	554.865171
11:00–12:00	511.263958	55.596218	523.653078
12:00–13:00	521.160865	56.137891	521.580743
13:00–14:00	506.491562	53.142982	551.805066
14:00–15:00	459.421302	48.577164	563.462838
15:00–16:00	378.430135	36.353455	617.887699
16:00–17:00	406.699563	4.627200	688.453229
17:00–18:00	414.054667	0.005527	763.773356
18:00–19:00	469.381573	0.000000	775.786919
19:00–20:00	543.795656	0.000000	759.480315
20:00–21:00	554.936594	0.000000	737.570371
21:00–22:00	556.811062	0.000000	696.002209
22:00–23:00	557.898688	0.000000	660.699636
23:00–24:00	517.122375	0.000000	622.535037

Table A1. *Cont.*

(**c**)						
Target interval (AEST)	Wind forecast (MW)	Actual wind output (MW)	PV forecast (MW)	Actual PV output (MW)	Load forecast (MW)	Actual load (MW)
2 June 2026						
00:00–00:15	338.686104	387.862603	0.000000	0.000000	598.599474	593.393908
00:15–00:30	355.024542	426.606699	0.000000	0.000000	585.667655	594.102252
00:30–00:45	384.477042	529.084207	0.000000	0.000000	574.115649	589.922202
00:45–01:00	473.659083	537.187805	0.000000	0.000000	578.175856	580.472554
01:00–01:15	477.733667	568.254808	0.000000	0.000000	564.461446	573.782033
01:15–01:30	584.789333	578.316441	0.000000	0.000000	572.638667	562.913953
01:30–01:45	563.925542	580.807615	0.000000	0.000000	556.098855	550.274142
01:45–02:00	597.850458	559.724694	0.000000	0.000000	549.861295	539.831119
02:00–02:15	578.132042	575.224281	0.000000	0.000000	537.377952	534.305141
02:15–02:30	598.391063	535.200660	0.000000	0.000000	527.575004	528.785891
02:30–02:45	580.049021	519.148587	0.000000	0.000000	518.878298	523.966014
02:45–03:00	550.173021	514.747813	0.000000	0.000000	518.958276	519.934211
03:00–03:15	542.902938	498.104423	0.000000	0.000000	514.066146	519.579915
03:15–03:30	564.477375	498.211079	0.000000	0.000000	515.055036	525.069267
03:30–03:45	555.064125	457.702769	0.000000	0.000000	513.486864	519.327273
03:45–04:00	505.177750	456.791629	0.000000	0.000000	520.524207	511.393475
04:00–04:15	510.994458	472.766177	0.000000	0.000000	526.169778	512.003901
04:15–04:30	455.301000	462.336191	0.000000	0.000000	516.165016	516.616482
04:30–04:45	467.946646	420.015269	0.000000	0.000000	524.238339	521.638920
04:45–05:00	488.796000	451.150117	0.000000	0.000000	521.988482	521.964065
05:00–05:15	494.725000	476.401160	0.000000	0.000000	541.450866	533.091016
05:15–05:30	449.707271	495.622948	0.000000	0.000000	541.998755	552.188887
05:30–05:45	464.353312	500.653749	0.000000	0.000000	567.469228	561.261566
05:45–06:00	521.861083	505.529490	0.000000	0.000000	569.002270	576.011210
06:00–06:15	520.494333	517.413462	0.000000	0.000000	613.731070	602.299405
06:15–06:30	551.778792	526.525166	0.000000	0.000000	609.411494	628.229068
06:30–06:45	543.318417	531.652927	0.000000	0.000000	656.714549	650.665848
06:45–07:00	610.807312	518.964418	0.000000	0.000000	658.250581	672.693267
07:00–07:15	589.467083	515.823786	0.034909	0.000000	690.600683	687.959157
07:15–07:30	597.656354	499.665053	0.457309	0.000000	689.434645	699.827588
07:30–07:45	577.697312	471.806527	9.541818	3.514793	698.960285	709.582699
07:45–08:00	566.763312	447.234025	14.425018	17.495118	696.377808	710.440784
08:00–08:15	552.577667	458.817520	40.612655	38.681094	681.684224	708.742802
08:15–08:30	438.421958	455.211616	37.609891	48.790553	703.536987	699.860477
08:30–08:45	453.024687	472.552920	68.628364	49.489571	674.576619	686.919688
08:45–09:00	474.087396	496.107631	71.572364	46.525322	674.737323	678.119085
09:00–09:15	480.956438	501.380768	87.423418	48.953484	657.911234	677.988778
09:15–09:30	512.606646	516.638029	94.470400	49.355547	672.124200	679.183220
09:30–09:45	511.004083	517.345627	93.376582	43.166887	652.929408	674.179468
09:45–10:00	522.873312	514.243757	84.188509	40.344545	665.768542	666.524224
10:00–10:15	522.496333	497.018787	82.071855	44.220668	647.934128	668.028365
10:15–10:30	528.030708	500.353283	78.877673	49.400219	651.497273	666.647306
10:30–10:45	529.291583	482.546696	83.126691	49.452779	632.552132	652.150554
10:45–11:00	512.439813	463.082567	98.024727	49.465920	659.501830	621.831552
11:00–11:15	519.050583	507.448763	91.973818	49.455408	639.439236	605.855325
11:15–11:30	470.564646	527.261874	84.558545	49.460662	593.866553	619.996286
11:30–11:45	490.860563	515.688063	79.568873	49.413362	588.689639	660.742366
11:45–12:00	548.626604	541.617626	83.824291	49.494825	629.012158	678.840385

Table A1. *Cont.*

(**c**)						
Target interval (AEST)	Wind forecast (MW)	Actual wind output (MW)	PV forecast (MW)	Actual PV output (MW)	Load forecast (MW)	Actual load (MW)
2 June 2026						
12:00–12:15	549.885875	535.811344	77.290473	49.526357	611.988739	677.483245
12:15–12:30	541.808896	533.262013	81.192727	46.199463	677.321295	673.393638
12:30–12:45	545.732687	542.238000	73.931636	37.516942	658.885175	671.563854
12:45–13:00	541.277917	534.502756	59.868509	10.034564	663.707792	667.599571
13:00–13:15	541.877875	545.824526	51.744000	25.060788	648.211435	670.404044
13:15–13:30	544.547208	536.945464	36.503855	8.087306	670.082138	671.444011
13:30–13:45	542.041500	537.420441	27.369891	17.274378	655.721921	676.019468
13:45–14:00	550.750521	524.799767	30.080582	31.864370	674.396481	678.084951
14:00–14:15	544.771792	546.958645	23.989527	34.655178	668.938523	672.015570
14:15–14:30	527.706667	538.418837	26.733964	43.868530	679.186957	662.853195
14:30–14:45	524.076437	510.036878	16.075636	15.876344	680.636284	654.443514
14:45–15:00	539.154000	513.865724	32.473600	11.992336	661.700860	667.405979
15:00–15:15	529.233833	512.780088	22.490182	16.972170	675.196264	671.679960
15:15–15:30	514.382458	526.544533	13.704727	10.828183	680.012154	673.366729
15:30–15:45	510.370438	517.762443	8.471855	11.619177	701.989743	672.081097
15:45–16:00	520.269750	508.107910	5.968873	13.390367	687.787988	679.846965
16:00–16:15	517.903604	505.296865	2.039273	15.211491	720.425116	700.424809
16:15–16:30	515.564729	508.156377	7.286109	12.799094	696.845718	718.135643
16:30–16:45	515.988229	506.867189	0.317673	10.123912	732.479415	734.551875
16:45–17:00	511.981021	517.171152	0.128000	3.567350	743.964898	751.938062
17:00–17:15	515.000063	514.117760	0.011636	0.000000	777.822628	768.430036
17:15–17:30	541.885896	519.245516	0.000582	0.000000	775.350028	789.207203
17:30–17:45	540.198313	527.000144	0.000000	0.000000	800.087990	795.443767
17:45–18:00	568.545542	532.544710	0.000000	0.000000	802.768384	804.385142
18:00–18:15	563.785979	553.094486	0.000000	0.000000	803.931433	799.080911
18:15–18:30	536.767000	565.976875	0.000000	0.000000	801.354936	801.641462
18:30–18:45	538.441750	576.755816	0.000000	0.000000	793.927418	791.621751
18:45–19:00	561.289896	574.119235	0.000000	0.000000	793.184442	788.309503
19:00–19:15	556.382750	569.107807	0.000000	0.000000	777.836830	775.891190
19:15–19:30	585.817604	581.486151	0.000000	0.000000	776.620711	771.919432
19:30–19:45	576.033792	573.208073	0.000000	0.000000	761.911431	763.658994
19:45–20:00	593.734167	582.184076	0.000000	0.000000	756.396665	755.232869
20:00–20:15	582.822625	572.471392	0.000000	0.000000	745.141401	748.055750
20:15–20:30	590.718333	560.335385	0.000000	0.000000	743.489513	742.126642
20:30–20:45	580.026562	542.325234	0.000000	0.000000	726.905600	731.325087
20:45–21:00	576.439646	544.205735	0.000000	0.000000	726.617081	720.507336
21:00–21:15	569.615521	560.907275	0.000000	0.000000	703.918192	705.784851
21:15–21:30	548.918563	555.624434	0.000000	0.000000	703.917444	693.549914
21:30–21:45	564.846333	577.269572	0.000000	0.000000	679.400731	674.815308
21:45–22:00	565.534521	570.765371	0.000000	0.000000	673.986873	663.056754
22:00–22:15	564.324979	574.506967	0.000000	0.000000	658.350741	652.344644
22:15–22:30	583.258958	580.953012	0.000000	0.000000	655.277182	647.806561
22:30–22:45	577.185583	566.636022	0.000000	0.000000	637.152753	635.642384
22:45–23:00	592.752417	575.263054	0.000000	0.000000	634.786293	624.446917
23:00–23:15	584.874354	574.681447	0.000000	0.000000	617.793519	611.439854
23:15–23:30	587.280604	565.482524	0.000000	0.000000	612.605394	602.497731
23:30–23:45	581.845688	573.731524	0.000000	0.000000	601.391240	595.637287
23:45–24:00	600.954521	582.154998	0.000000	0.000000	594.033236	585.514426

Table A1. *Cont.*

(**c**)						
Target interval (AEST)	Wind forecast (MW)	Actual wind output (MW)	PV forecast (MW)	Actual PV output (MW)	Load forecast (MW)	Actual load (MW)
3 June 2026						
00:00–00:15	593.629896	573.993217	0.000000	0.000000	591.713118	583.810465
00:15–00:30	599.027917	562.380649	0.000000	0.000000	579.865117	588.360258
00:30–00:45	592.802146	559.201249	0.000000	0.000000	568.994048	579.680993
00:45–01:00	589.876146	556.545300	0.000000	0.000000	575.557501	578.441952
01:00–01:15	586.768875	545.940833	0.000000	0.000000	562.032198	565.329995
01:15–01:30	588.233479	571.967320	0.000000	0.000000	565.691019	551.314857
01:30–01:45	585.923479	584.927265	0.000000	0.000000	548.618267	543.463778
01:45–02:00	569.816042	575.485995	0.000000	0.000000	538.810835	538.033974
02:00–02:15	572.036208	568.245119	0.000000	0.000000	526.918734	527.764112
02:15–02:30	592.112354	537.536759	0.000000	0.000000	527.267050	526.399248
02:30–02:45	590.285208	572.723401	0.000000	0.000000	516.735328	524.051972
02:45–03:00	558.205083	590.200417	0.000000	0.000000	517.809429	518.761445
03:00–03:15	563.651229	590.626917	0.000000	0.000000	511.881318	508.774871
03:15–03:30	602.148021	592.148758	0.000000	0.000000	515.796517	503.868538
03:30–03:45	599.164271	589.832063	0.000000	0.000000	513.770899	505.033331
03:45–04:00	604.501333	588.465313	0.000000	0.000000	505.307400	502.238326
04:00–04:15	597.826396	589.948398	0.000000	0.000000	509.715924	500.109807
04:15–04:30	598.846646	588.785190	0.000000	0.000000	508.001996	502.318305
04:30–04:45	591.231667	582.261600	0.000000	0.000000	514.065398	506.588548
04:45–05:00	597.868104	587.176093	0.000000	0.000000	510.340054	512.907831
05:00–05:15	588.300854	586.691437	0.000000	0.000000	528.208851	525.396405
05:15–05:30	591.597417	581.583085	0.000000	0.000000	529.344991	535.582551
05:30–05:45	581.208833	578.539388	0.000000	0.000000	552.224018	547.815993
05:45–06:00	594.523417	580.662219	0.000000	0.000000	552.685949	559.625375
06:00–06:15	581.699708	569.611869	0.000000	0.000000	593.535428	585.290686
06:15–06:30	610.191312	580.167868	0.000000	0.000000	592.195230	612.974141
06:30–06:45	596.944104	584.093644	0.000000	0.000000	633.113475	634.737458
06:45–07:00	605.545646	582.629959	0.000000	0.000000	637.991404	657.713655
07:00–07:15	592.205396	582.397307	0.029091	0.000000	665.613070	666.630862
07:15–07:30	599.748187	583.957937	0.001164	0.000000	674.737323	676.720586
07:30–07:45	588.887979	581.961113	3.955200	0.948666	683.070763	671.802294
07:45–08:00	583.658396	570.203148	9.740218	3.023377	673.007699	655.737120
08:00–08:15	577.568979	576.862440	22.304000	7.164918	655.802647	636.784006
08:15–08:30	545.548208	574.099862	14.649018	8.620765	635.634661	622.360006
08:30–08:45	541.330854	574.555434	24.745309	13.837106	605.489568	599.577900
08:45–09:00	547.508500	585.353770	26.398836	22.745623	590.852043	576.311689
09:00–09:15	543.765979	595.056770	29.614545	15.942039	570.408244	564.426564
09:15–09:30	553.556208	587.030707	28.513164	26.224937	568.915565	552.231991
09:30–09:45	549.600333	569.912350	27.001600	24.133143	548.586127	543.987748
09:45–10:00	563.521292	557.660020	32.519564	35.745751	534.382129	536.755317
10:00–10:15	557.111042	565.744239	33.099636	22.974251	515.023643	527.337063
10:15–10:30	545.994167	563.640807	37.560436	28.823913	516.706925	517.842816
10:30–10:45	543.013625	557.795737	41.396945	43.424421	503.330367	509.386543
10:45–11:00	547.418667	555.081616	42.068945	49.442269	503.981405	498.538396
11:00–11:15	544.338667	554.936214	43.828945	49.455408	486.348805	504.904768
11:15–11:30	536.041917	578.965888	78.013673	46.830154	482.959071	499.746292
11:30–11:45	535.326458	569.485835	66.230109	48.356951	477.193158	490.959891
11:45–12:00	538.666333	588.077602	60.267055	49.481687	489.554665	489.990933

Table A1. *Cont.*

(**c**)						
Target interval (AEST)	Wind forecast (MW)	Actual wind output (MW)	PV forecast (MW)	Actual PV output (MW)	Load forecast (MW)	Actual load (MW)
3 June 2026						
12:00–12:15	537.509729	582.474863	59.080727	39.306531	486.978915	490.997015
12:15–12:30	553.129500	586.953167	73.552873	40.076499	491.624384	487.769230
12:30–12:45	549.338854	589.473420	65.988655	49.434385	483.904609	480.640697
12:45–13:00	555.136313	579.634729	64.245527	49.444897	481.070237	482.397479
13:00–13:15	550.715229	585.111455	58.434327	49.418618	482.923193	486.709580
13:15–13:30	549.840958	583.095248	81.428364	49.458036	487.545490	490.633500
13:30–13:45	546.724063	587.486290	72.354327	44.591199	492.377824	498.107360
13:45–14:00	555.134708	587.757710	87.003927	32.358414	495.863234	504.803612
14:00–14:15	551.247813	586.167986	78.533818	49.397593	508.425059	505.112313
14:15–14:30	555.295125	578.936804	55.179636	49.542125	515.862294	514.782711
14:30–14:45	551.706604	570.115914	54.494255	49.402849	540.261656	526.361128
14:45–15:00	549.260250	570.367934	80.418327	49.479057	531.172533	541.561490
15:00–15:15	581.964396	561.188390	70.650182	49.182107	564.491344	554.517726
15:15–15:30	571.258187	570.290404	72.186764	28.592659	561.281000	573.750888
15:30–15:45	572.188604	571.056180	51.346036	49.279341	602.941474	598.576552
15:45–16:00	577.039604	570.348545	48.734836	32.768365	600.358249	619.478545
16:00–16:15	575.595854	554.916830	20.409600	21.770680	643.127955	641.020614
16:15–16:30	587.237292	549.488592	25.296291	14.052592	641.061973	662.051668
16:30–16:45	583.137042	557.999301	1.393455	3.320328	684.748065	680.604641
16:45–17:00	557.143125	559.172187	1.000145	1.409860	689.605813	700.639580
17:00–17:15	558.575646	564.047908	0.009891	0.363962	726.602879	714.783780
17:15–17:30	570.311729	572.723423	0.000582	0.000000	718.896558	732.032932
17:30–17:45	568.794187	570.561813	0.000000	0.000000	747.933914	744.239714
17:45–18:00	585.958771	575.951268	0.000000	0.000000	744.281821	749.572847
18:00–18:15	581.526458	576.232388	0.000000	0.000000	746.775350	748.478315
18:15–18:30	584.746021	591.353926	0.000000	0.000000	746.598949	745.755315
18:30–18:45	580.557542	597.111729	0.000000	0.000000	742.002066	743.647227
18:45–19:00	597.770250	593.292582	0.000000	0.000000	742.162022	735.649646
19:00–19:15	592.858292	597.741787	0.000000	0.000000	729.397635	725.328458
19:15–19:30	611.294979	591.935527	0.000000	0.000000	720.233018	719.444198
19:30–19:45	604.746771	596.888771	0.000000	0.000000	710.331405	713.770223
19:45–20:00	611.655917	598.400950	0.000000	0.000000	708.373058	709.949702
20:00–20:15	607.722500	585.906293	0.000000	0.000000	698.120139	704.712992
20:15–20:30	610.183292	588.155137	0.000000	0.000000	698.382497	702.321367
20:30–20:45	606.233833	597.538229	0.000000	0.000000	685.101614	691.656845
20:45–21:00	606.020479	602.375192	0.000000	0.000000	688.246182	682.548538
21:00–21:15	603.704062	594.911368	0.000000	0.000000	668.851817	673.994098
21:15–21:30	611.517958	584.927265	0.000000	0.000000	665.613817	665.252046
21:30–21:45	609.212771	577.521603	0.000000	0.000000	645.405468	653.500219
21:45–22:00	592.460458	544.409282	0.000000	0.000000	648.467815	638.862944
22:00–22:15	592.779688	517.297149	0.000000	0.000000	636.859749	635.255947
22:15–22:30	561.442292	530.819311	0.000000	0.000000	632.877278	629.722744
22:30–22:45	570.545938	570.348550	0.000000	0.000000	618.603019	620.407141
22:45–23:00	539.729896	581.806043	0.000000	0.000000	616.738852	609.667624
23:00–23:15	553.135917	580.991784	0.000000	0.000000	602.498230	599.664606
23:15–23:30	611.359146	593.098703	0.000000	0.000000	600.332836	592.483501
23:30–23:45	609.840000	590.791703	0.000000	0.000000	589.461766	584.810069
23:45–24:00	608.932042	585.344070	0.000000	0.000000	585.192270	575.766292

Table A1. *Cont.*

(**c**)						
Target interval (AEST)	Wind forecast (MW)	Actual wind output (MW)	PV forecast (MW)	Actual PV output (MW)	Load forecast (MW)	Actual load (MW)
4 June 2026						
00:00–00:15	606.782458	576.135453	0.000000	0.000000	584.963547	575.383343
00:15–00:30	596.469271	561.236846	0.000000	0.000000	572.253724	580.174068
00:30–00:45	595.962354	565.783012	0.000000	0.000000	562.097975	572.003325
00:45–01:00	578.853917	572.490765	0.000000	0.000000	568.513431	565.127433
01:00–01:15	581.224875	575.495706	0.000000	0.000000	555.311779	558.269730
01:15–01:30	576.952979	576.707344	0.000000	0.000000	557.394204	543.817825
01:30–01:45	579.234104	574.439116	0.000000	0.000000	541.265496	537.600446
01:45–02:00	587.245312	581.835105	0.000000	0.000000	535.030925	535.522256
02:00–02:15	586.197792	581.137175	0.000000	0.000000	523.207591	535.731296
02:15–02:30	589.497562	581.844800	0.000000	0.000000	524.662897	524.388081
02:30–02:45	587.258146	582.639638	0.000000	0.000000	513.936088	516.102727
02:45–03:00	588.565542	579.004655	0.000000	0.000000	517.037302	514.009090
03:00–03:15	585.169521	564.367789	0.000000	0.000000	512.443408	514.424678
03:15–03:30	583.125812	572.015798	0.000000	0.000000	509.416192	516.810323
03:30–03:45	579.720167	573.867226	0.000000	0.000000	507.714224	509.523827
03:45–04:00	574.711958	569.534323	0.000000	0.000000	516.360103	508.285035
04:00–04:15	571.980063	583.250339	0.000000	0.000000	520.196072	508.211285
04:15–04:30	568.928937	578.752651	0.000000	0.000000	513.234222	509.595334
04:30–04:45	564.581646	575.427834	0.000000	0.000000	520.393401	509.317527
04:45–05:00	582.394312	562.235274	0.000000	0.000000	515.163418	513.473908
05:00–05:15	573.860146	555.663222	0.000000	0.000000	533.722122	524.183027
05:15–05:30	563.803625	566.005953	0.000000	0.000000	531.419195	536.308336
05:30–05:45	558.655854	566.122271	0.000000	0.000000	553.907300	548.819085
05:45–06:00	559.097000	582.533009	0.000000	0.000000	552.999882	567.611246
06:00–06:15	553.671708	581.757555	0.000000	0.000000	595.294203	591.996904
06:15–06:30	576.980250	585.557339	0.000000	0.000000	603.334638	613.382504
06:30–06:45	566.447292	579.072506	0.000000	0.000000	647.078285	636.304136
06:45–07:00	583.850896	579.440865	0.000000	0.000000	639.910884	658.673644
07:00–07:15	569.472750	567.857392	0.023855	0.000000	667.554973	656.991608
07:15–07:30	572.555958	580.574979	0.001164	0.000000	673.130283	666.295501
07:30–07:45	558.237167	573.305003	2.488436	1.341535	679.703453	667.923222
07:45–08:00	567.005542	564.997847	4.238545	4.523896	688.659528	660.359666
08:00–08:15	552.455750	539.446338	9.108945	6.176832	669.058116	661.058542
08:15–08:30	558.862792	511.277620	10.242327	11.979196	657.257206	648.626525
08:30–08:45	544.430104	519.003153	18.927127	22.477582	624.095361	631.435675
08:45–09:00	510.468292	461.725511	19.422836	51.783709	610.536423	607.704543
09:00–09:15	508.031563	507.778350	17.857745	31.522748	588.384675	601.613485
09:15–09:30	481.298125	512.906085	40.852945	44.273226	590.383385	595.057258
09:30–09:45	481.995937	481.267181	35.503127	31.265214	569.947060	591.533478
09:45–10:00	516.548083	450.248645	40.581236	46.514810	575.856485	577.889080
10:00–10:15	510.107354	483.263988	43.112145	49.460664	558.202209	565.006594
10:15–10:30	485.167375	477.525580	55.639855	49.076992	563.784246	547.768155
10:30–10:45	493.104792	509.319575	50.701382	27.896270	549.037593	537.285516
10:45–11:00	509.760854	532.525337	59.124945	42.496778	536.359911	533.105217
11:00–11:15	511.464479	531.051932	54.822400	52.251473	522.502735	537.206285
11:15–11:30	550.060729	527.804681	47.199418	46.396554	519.432914	538.732600
11:30–11:45	539.085021	513.080575	48.868073	48.774786	515.082692	546.668641
11:45–12:00	531.439562	502.224094	58.831709	57.254957	538.674049	548.425173

Table A1. *Cont.*

(**c**)						
Target interval (AEST)	Wind forecast (MW)	Actual wind output (MW)	PV forecast (MW)	Actual PV output (MW)	Load forecast (MW)	Actual load (MW)
4 June 2026						
12:00–12:15	524.488708	545.000594	54.118400	44.917058	530.078250	552.163723
12:15–12:30	514.797937	485.474060	65.117091	42.349616	544.005687	568.399817
12:30–12:45	512.255333	479.066804	62.525091	49.741847	532.162918	570.263486
12:45–13:00	518.426563	476.439928	58.617600	25.715128	575.481260	567.226552
13:00–13:15	511.717938	475.858321	54.060800	26.427285	563.645966	558.596869
13:15–13:30	479.588083	465.360505	54.308073	63.430480	562.210094	542.661752
13:30–13:45	478.628792	451.276135	50.925964	49.232035	561.607641	525.363517
13:45–14:00	464.249042	383.229209	64.941964	60.489879	543.078836	526.139132
14:00–14:15	463.132542	367.690865	53.504582	49.523733	551.301652	533.328957
14:15–14:30	401.341646	357.415975	67.031855	31.979997	536.012341	545.286087
14:30–14:45	409.471562	337.156986	50.514618	17.542419	557.353841	549.891193
14:45–15:00	363.380646	339.095648	51.403636	16.351988	559.090940	562.969265
15:00–15:15	377.593563	390.567036	42.023564	19.826050	593.446480	582.852967
15:15–15:30	350.611479	353.170312	38.893964	47.368869	580.956410	599.362881
15:30–15:45	363.318083	339.463981	26.835782	13.605855	623.507857	622.179619
15:45–16:00	385.447563	306.991455	27.191273	5.806301	615.974200	642.961769
16:00–16:15	400.080771	328.849835	8.418909	4.318922	661.411593	668.319376
16:15–16:30	321.811875	365.277241	5.444655	4.195411	667.550488	682.209440
16:30–16:45	351.845083	391.904708	0.778473	5.782652	711.162582	705.625641
16:45–17:00	383.023667	431.443646	0.529455	2.994471	707.171141	734.185619
17:00–17:15	404.033437	413.394734	0.011055	0.000000	747.689495	750.997258
17:15–17:30	449.574125	444.694378	0.000582	0.000000	761.331401	763.795779
17:30–17:45	461.082417	480.346319	0.000000	0.000000	785.448970	778.199348
17:45–18:00	445.988812	502.398569	0.000000	0.000000	774.322269	783.998897
18:00–18:15	461.529979	529.375005	0.000000	0.000000	776.177467	784.243565
18:15–18:30	514.584583	556.080012	0.000000	0.000000	778.039392	783.226520
18:30–18:45	517.290812	574.342203	0.000000	0.000000	773.000759	781.706434
18:45–19:00	555.911125	578.490937	0.000000	0.000000	778.048361	780.457178
19:00–19:15	547.697792	578.558755	0.000000	0.000000	764.941637	771.655329
19:15–19:30	588.987438	569.165969	0.000000	0.000000	765.797479	766.685712
19:30–19:45	574.150500	552.551674	0.000000	0.000000	755.217920	761.379986
19:45–20:00	566.206667	564.387183	0.000000	0.000000	755.874938	757.770249
20:00–20:15	557.879437	570.542408	0.000000	0.000000	744.732540	751.330874
20:15–20:30	556.270458	564.425935	0.000000	0.000000	744.698904	745.907299
20:30–20:45	551.398604	553.714860	0.000000	0.000000	728.692779	738.818630
20:45–21:00	564.270437	551.068606	0.000000	0.000000	730.059885	729.425291
21:00–21:15	558.736063	558.726309	0.000000	0.000000	708.038943	721.188273
21:15–21:30	549.303562	572.907586	0.000000	0.000000	711.072886	702.355251
21:30–21:45	548.010604	579.043433	0.000000	0.000000	686.198139	690.455925
21:45–22:00	577.280229	573.750891	0.000000	0.000000	685.111331	678.269076
22:00–22:15	564.859167	567.547178	0.000000	0.000000	669.582834	665.622538
22:15–22:30	564.669875	571.540836	0.000000	0.000000	669.585076	659.312225
22:30–22:45	540.456583	550.787486	0.000000	0.000000	652.355358	649.641079
22:45–23:00	555.503667	549.314107	0.000000	0.000000	647.921421	633.853462
23:00–23:15	528.880917	568.497123	0.000000	0.000000	629.833617	626.089337
23:15–23:30	530.884521	565.501908	0.000000	0.000000	624.630543	617.127034
23:30–23:45	508.585000	557.611558	0.000000	0.000000	611.911751	607.159893
23:45–24:00	556.525521	554.645427	0.000000	0.000000	610.962475	599.528817

Appendix A.2. Bid Discretization

Medium- and long-term bids divide declared contract energy into blocks; day-ahead bids divide hourly output ranges. Prices are discretized on the corresponding grid and assigned to power or energy blocks in non-decreasing order.

Monthly contracting and weekly supplementary trading determine each participant's declared energy Qbid separately. Sellers divide this energy into three blocks and assign selected prices from lowest to highest, forming stepwise bid curves.

Table A2. (**a**) Medium- and long-term contract-bid discretization. (**b**) Day-ahead bid discretization.

(**a**)		
Participant	Power blocks (MW)	Price blocks and bid curves
thermal	Cumulative breakpoints: Qmin, Qlow, Qhigh, Qbid.	Select three non-decreasing prices from Gth.
hydro, renewable	Cumulative breakpoints: Qmin, Qlow, Qhigh, Qbid.	Select three non-decreasing prices from Ghr.
user	Declared procurement quantity: Qbid.	Procurement enters the clearing balance.
(**b**)		
Participant	Power blocks (MW)	Price blocks and bid curves
thermal A	Cumulative breakpoints: Pmin, Plow, Phigh, Pmax.	Select three non-decreasing prices from GDA, each no lower than $p_{floor,A}$.
thermal B	Cumulative breakpoints: Pmin, Plow, Phigh, Pmax.	Select three non-decreasing prices from GDA, each no lower than $p_{floor,B}$.
thermal C	Cumulative breakpoints: Pmin, Plow, Phigh, Pmax.	Select three non-decreasing prices from GDA, each no lower than $p_{floor,C}$.
hydro	Cumulative breakpoints: Pmin, Plow, Phigh, Pmax.	Select three non-decreasing prices from GDA.
renewable wind, renewable solar	Upper endpoint: hourly forecast $\hat{P}h$. Cumulative breakpoints: Pmin, Plow, Phigh, $\hat{P}h$.	Select three non-decreasing prices from GDA.

Code identifiers: thermal includes thermal1, thermal2, and thermal3; hydro denotes hydro1; renewable includes renewable1 and renewable2.

Energy blocks: Qmin = 0, Qlow = 0.3Qbid, Qhigh = 0.7Qbid, and the endpoint is Qbid. The three blocks therefore contain 30%, 40%, and 30% of declared energy, respectively. Equal prices across blocks are allowed.

Price basis: thermal bids use a benchmark of 364.4 CNY/MWh with ±20% variation, giving a nominal range of 291.52–437.28 CNY/MWh. Hydropower and renewable bids use a nominal range of 0–437.28 CNY/MWh. Both grids use 10-CNY/MWh increments.

Implemented grids: Gth = {291.52, 301.52, ..., 441.52} CNY/MWh contains 16 levels; Ghr = {0, 10, ..., 440} CNY/MWh contains 45 levels.

At day-ahead gate closure, each generator submits bids for all 24 operating-day hours. Three non-decreasing prices are selected from GDA and assigned to the corresponding power blocks.

Code identifiers: thermal A, thermal B, and thermal C denote thermal1, thermal2, and thermal3, respectively. hydro denotes hydro1; renewable wind and renewable solar denote renewable1 and renewable2, respectively.

Power blocks: thermal bids extend from minimum stable output Pmin to maximum output Pmax. Hydropower bids extend from zero to Pmax. Wind and photovoltaic bids extend from zero to hourly day-ahead forecast power $\hat{P}h$. Intermediate breakpoints Plow

and Phigh lie at 30% and 70% of the output range. $\hat{P}h$ is the mean of the four 15 min day-ahead forecasts within the hour.

Fixed breakpoints are 236.40, 342.78, 484.62, and 591.00 MW for thermal1; 124.00, 179.80, 254.20, and 310.00 MW for thermal2; 160.00, 232.00, 328.00, and 400.00 MW for thermal3; and 0, 30.00, 70.00, and 100.00 MW for hydro1.

Day-ahead prices use GDA = {0, 50, ..., 600} CNY/MWh, containing 13 levels. Each thermal block's minimum bid is based on marginal generation cost 2aqk + b at its endpoint qk, using a and b from Table A3. This value is rounded upward to the first grid point at or above it.

For example, thermal1's first block ends at 342.78 MW, where marginal cost is approximately 283.41 CNY/MWh; its minimum bid is therefore 300 CNY/MWh. The same rule gives 300 CNY/MWh for all three blocks of thermal1 and thermal2, and 350 CNY/MWh for all three blocks of thermal3.

Intraday and real-time clearing retain the frozen day-ahead power breakpoints and block prices for the corresponding hour.

Appendix A.3. Unit and Storage Technical and Economic Parameters

Table A3 lists equipment output and operating limits, cost parameters, and storage ratings. Renewable delivery limits before the slash apply to joint operation in Section 4.2. Storage costs and capacities are reported per system.

Appendix A.4. Generator and Storage Initialization

Table A4 lists physical initial states for the single-day case and the first day of continuous operation. Each storage system in Section 4.2 starts at 50% SOC, corresponding to 300 MWh.

The table gives initial physical states for the single-day case or the first day of continuous operation. Thermal units begin with eight hours offline, equivalent to 32 15 min intervals, satisfying minimum down time. For later days, day-ahead planning states are inferred from the intraday schedule available at gate closure. Actual operation carries forward the preceding day's terminal states, including thermal commitment and durations, thermal and hydropower output, and storage energy.

Wind and photovoltaic plants are initialized using their actual output values.

Table A3. Unit and storage technical and economic parameters.

Unit/ Equip-ment	Type/ Scenario	Installed Capacity or Maxi-mum Output (MW)	Mini-mum Output (MW)	Deliv-ery Limit (MW)	Up/ Down Ramp Rate (MW/h)	Mini-mum Up/ Down time (h)	Annual Utiliza-tion (h)	Auxil-iary Con-sump-tion	Fuel Co-efficient a [CNY/ (MW^2·h)]	Fuel Co-efficient b (CNY/ MWh)	Fixed Cost: Thermal, Cost-Function Constant and Other O&M; Wind/PV, Plant O&M and Allocated Construction Investment; Hydro, Fixed O&M; Storage, Fixed O&M and Depreciation.	Start-Up Cost (CNY/ Event)	Shut-down Cost (CNY/ Event)	Storage Power (MW)	Storage Capac-ity (MWh)	Rated Duration (h)	Charge/ Dis-charge Effi-ciency	Charge/ Dis-charge Variable Cost (CNY/ MWh)
thermal1	Thermal	591	236.4	—	62.8	8/8	4346	5.7%	0.02	269.70	8770.55 CNY/h	180,000	0	—	—	—	—	—
thermal2	Thermal	310	124	—	118.2	8/8	4346	5.7%	0.04	269.70	4600.46 CNY/h	120,000	0	—	—	—	—	—
thermal3	Thermal	400	160	—	120	8/8	4346	5.7%	0.03	296.70	5936.07 CNY/h	60,000	0	—	—	—	—	—
hydro1	Hy-dropower	100	0	—	24	—	3367	0.5%	—	—	1712.33 CNY/h	—	—	—	—	—	—	—
renew-able1	Wind	616	0	716/616	—	—	—	—	—	—	16,016 (CNY 10,000/year)	—	—	—	—	—	—	—
renew-able2	Photo-voltaic	160	0	260/160	—	—	—	—	—	—	3.10 (CNY 10,000/day)	—	—	—	—	—	—	—
Storage associ-ated with re-newable1	Joint op-eration	—	—	—	—	—	—	—	—	—	449.70 (CNY 10,000/year); 12,320.55 CNY/day	—	—	100	600	6	95%/95%	6.3/6.0
Storage associ-ated with re-newable2	Joint op-eration	—	—	—	—	—	—	—	—	—	449.70 (CNY 10,000/year); 12,320.55 CNY/day	—	—	100	600	6	95%/95%	6.3/6.0
storage1	Indepen-dent participa-tion	—	—	—	—	—	—	—	—	—	449.70 (CNY 10,000/year); 12,320.55 CNY/day	—	—	100	600	6	95%/95%	6.3/6.0
storage2	Indepen-dent participa-tion	—	—	—	—	—	—	—	—	—	449.70 (CNY 10,000/year); 12,320.55 CNY/day	—	—	100	600	6	95%/95%	6.3/6.0

Table A4. Generator and storage initialization.

Unit/Equipment	Applicable Case	Initial Commitment	Initial Offline Duration (h)	Previous Output (MW)	Initial SOC	Initial Storage Energy (MWh)
thermal1	All scenarios	Offline	8	0	—	—
thermal2	All scenarios	Offline	8	0	—	—
thermal3	All scenarios	Offline	8	0	—	—
hydro1	All scenarios	Online	—	13	—	—
renewable1	Wind plant	—	—	—	—	—
renewable2	PV plant	—	—	—	—	—
Storage associated with renewable1	Section 4.2 joint operation	—	—	—	50%	300
Storage associated with renewable2	Section 4.2 joint operation	—	—	—	50%	300
storage1	Section 4.2 independent participation	—	—	—	50%	300
storage2	Section 4.2 independent participation	—	—	—	50%	300

References

1. Cheng, Y.S.; Chung, M.K.; Tsang, K.P. Electricity market reforms for energy transition: Lessons from China. *Energies* **2023**, *16*, 905. [CrossRef]
2. Liu, P.; Gao, P.; Zhang, C. How to promote energy transition with market design: A review on China's electric power sector. *Front. Energy Res.* **2021**, *9*, 709272. [CrossRef]
3. Fan, Y.; Ding, T.; Sun, Y.; He, Y.; Wang, C.; Wang, Y.; Chen, T.; Liu, J. Review and cogitation for worldwide spot market development to promote renewable energy accommodation. *Proc. CSEE* **2021**, *41*, 1729–1751. (In Chinese) [CrossRef]
4. Liu, S.; Huang, Y.; Wang, Y.; Shao, Q.; Zhou, H.; Wang, J.; Chen, C. Incentive mechanisms to integrate more renewable energy in electricity markets in China. *Energies* **2023**, *16*, 6573. [CrossRef]
5. Cramton, P. Electricity market design. *Oxf. Rev. Econ. Policy* **2017**, *33*, 589–612. [CrossRef]
6. Liao, Z.; Tao, W.; Wang, B.; Liu, Y. Bidding strategy for wind and thermal power joint participation in the electricity spot market considering uncertainty. *Energies* **2024**, *17*, 1714. [CrossRef]
7. Zhang, L.; Zhu, J.; Zou, J.; Xuan, P.; Xie, P.; Li, X. Wind and thermal power joint bidding strategy considering penalties for wind power's bidding deviation. *South. Power Syst. Technol.* **2018**, *12*, 71–77, 85. (In Chinese)
8. Ortner, A.; Totschnig, G. The future relevance of electricity balancing markets in Europe: A 2030 case study. *Energy Strategy Rev.* **2019**, *24*, 111–120. [CrossRef]
9. Gaudard, L.; Gabbi, J.; Bauder, A.; Romerio, F. Long-term uncertainty of hydropower revenue due to climate change and electricity prices. *Water Resour. Manag.* **2016**, *30*, 1325–1343. [CrossRef]
10. Zhang, X.; Liu, Z.; Chen, X.; Zhan, S.; Cheng, Y.; He, Z.; Yang, Q. Multi-agent reinforcement learning-based trading strategy for energy storage in energy and frequency-regulation markets. *Electr. Power Autom. Equip.* **2026**, *46*, 139–148. (In Chinese) [CrossRef]
11. Liu, J.; Wu, T.; Peng, J.; Sun, S.; Yuan, Y. Research prospects on the optimization of multi-agent bidding strategies in electricity spot markets. *Power Syst. Technol.* **2025**, *49*, 4997–5008. (In Chinese) [CrossRef]
12. Li, T.; Shahidehpour, M. Strategic bidding of transmission-constrained GENCOs with incomplete information. *IEEE Trans. Power Syst.* **2005**, *20*, 437–447. [CrossRef]
13. Abapour, S.; Nazari-Heris, M.; Mohammadi-Ivatloo, B.; Tarafdar Hagh, M. Game theory approaches for the solution of power system problems: A comprehensive review. *Arch. Comput. Methods Eng.* **2020**, *27*, 81–103. [CrossRef]
14. Zhang, G.; Zhang, G.; Gao, Y.; Lu, J. Competitive strategic bidding optimization in electricity markets using bilevel programming and swarm technique. *IEEE Trans. Ind. Electron.* **2011**, *58*, 2138–2146. [CrossRef]

15. David, A.K.; Wen, F. Market power in electricity supply. *IEEE Trans. Energy Convers.* **2001**, *16*, 352–360. [CrossRef]
16. Huang, W.; Li, H. Game theory applications in the electricity market and renewable energy trading: A critical survey. *Front. Energy Res.* **2022**, *10*, 1009217. [CrossRef]
17. Jia, H.; Guo, Y.; Ma, Q.; Yang, Z.; Zheng, Y.; Zeng, D.; Liu, D. Review of spot electricity price prediction studies based on machine-learning methods. *Electr. Power Constr.* **2025**, *46*, 160–179. (In Chinese) [CrossRef]
18. Weron, R. Electricity price forecasting: A review of the state-of-the-art with a look into the future. *Int. J. Forecast.* **2014**, *30*, 1030–1081. [CrossRef]
19. Lago, J.; Marcjasz, G.; De Schutter, B.; Weron, R. Forecasting day-ahead electricity prices: A review of state-of-the-art algorithms, best practices and an open-access benchmark. *Appl. Energy* **2021**, *293*, 116983. [CrossRef]
20. Motamedi, A.; Zareipour, H.; Rosehart, W.D. Electricity price and demand forecasting in smart grids. *IEEE Trans. Smart Grid* **2012**, *3*, 664–674. [CrossRef]
21. Cao, D.; Hu, W.; Zhao, J.; Zhang, G.; Zhang, B.; Liu, Z.; Chen, Z.; Blaabjerg, F. Reinforcement learning and its applications in modern power and energy systems: A review. *J. Mod. Power Syst. Clean Energy* **2020**, *8*, 1029–1042. [CrossRef]
22. Wu, F.; Yang, Y.; Xu, Q.; Zhao, Y. Optimization model for medium- and long-term bilateral bidding based on DDPG and electricity-price perception. *Power Demand Side Manag.* **2026**, *28*, 113–119. (In Chinese)
23. Dou, C.; Jia, X.; Li, H. Multi-agent-system-based market bidding strategy for distributed generation in a microgrid. *Power Syst. Technol.* **2016**, *40*, 579–586. (In Chinese)
24. Esmaeili Aliabadi, D.; Kaya, M.; Sahin, G. Competition, risk and learning in electricity markets: An agent-based simulation study. *Appl. Energy* **2017**, *195*, 1000–1011. [CrossRef]
25. Gronauer, S.; Diepold, K. Multi-agent deep reinforcement learning: A survey. *Artif. Intell. Rev.* **2022**, *55*, 895–943. [CrossRef]
26. Du, Y.; Li, F.; Zandi, H.; Xue, Y. Approximating Nash equilibrium in day-ahead electricity market bidding with multi-agent deep reinforcement learning. *J. Mod. Power Syst. Clean Energy* **2021**, *9*, 534–544. [CrossRef]
27. Li, P. Research on Auxiliary Bidding Technology for Electricity-Market Generators Based on Multi-Agent Reinforcement Learning. Master's Thesis, Sichuan University, Chengdu, China, 2023. (In Chinese)
28. Wu, J.; Wang, J.; Kong, X. Strategic bidding in a competitive electricity market: An intelligent method using multi-agent transfer learning based on reinforcement learning. *Energy* **2022**, *256*, 124657. [CrossRef]
29. Ge, X.; Fan, W.; Fu, Y.; Li, Y. Joint bidding model for wind-thermal-storage multi-agent games in energy and frequency-regulation markets based on improved policy hill climbing. *Power Syst. Technol.* **2023**, *47*, 1920–1930. (In Chinese) [CrossRef]
30. Zhang, S.; Wang, Y.; Li, Y.; He, Y. Two-stage day-ahead bidding decision model for a wind power generator's spot-price forecasting based on Informer and MATD3. *Electr. Power Constr.* **2026**, *47*, 63–81. (In Chinese) [CrossRef]
31. Eltamaly, A.M. A novel musical chairs algorithm applied for MPPT of PV systems. *Renew. Sustain. Energy Rev.* **2021**, *146*, 111135. [CrossRef]
32. Eltamaly, A.M.; Almutairi, Z.A. A novel star-nosed mole optimization algorithm applied for MPPT of PV systems. *Sci. Rep.* **2025**, *15*, 17807. [CrossRef] [PubMed]
33. Wang, T. Research on Multi-Agent-Based Generator Bidding Strategies in Medium- and Long-Term Electricity Markets. Master's Thesis, North China Electric Power University, Beijing, China, 2024. (In Chinese)
34. Han, O.; Ding, T.; Bai, L.; He, Y.; Li, F.; Shahidehpour, M. Evolutionary game-based demand-response bidding strategy for end-users using Q-learning and compound differential evolution. *IEEE Trans. Cloud Comput.* **2022**, *10*, 97–110. [CrossRef]
35. Zhou, F.; Wang, H.; Wang, H.; Wang, M.; Jin, Y.; Li, Z.; Zhang, Z.; Wang, P. Multi-market participant behavior in coupled electricity-carbon-green-certificate markets based on multi-agent reinforcement learning. *Electr. Power* **2025**, *58*, 44–55. (In Chinese) [CrossRef]
36. Yin, B.; Weng, H.; Hu, Y.; Xi, J.; Ding, P.; Liu, J. Multi-agent deep reinforcement learning for simulating a centralized double-sided auction electricity market. *IEEE Trans. Power Syst.* **2025**, *40*, 518–529. [CrossRef]
37. Cheng, L.; Yu, F.; Huang, P.; Liu, G.; Zhang, M.; Sun, R. Game-theoretic evolution in renewable energy systems: Advancing sustainable energy management and decision optimization in decentralized power markets. *Renew. Sustain. Energy Rev.* **2025**, *217*, 115776. [CrossRef]
38. Stoft, S. *Power System Economics: Designing Markets for Electricity*; IEEE Press: Piscataway, NJ, USA; Wiley-Interscience: New York, NY, USA, 2002.
39. Hebei Provincial Development and Reform Commission. Work Plan for Continuous Trial Operation of the Southern Hebei Power Grid Electricity Spot Market; Document No. 702 (2024). 22 May 2024. Available online: https://cpnn.com.cn/news/dfny/202405/t20240528_1704621.html (accessed on 7 November 2026). (In Chinese)

Disclaimer/Publisher's Note: The statements, opinions and data contained in all publications are solely those of the individual author(s) and contributor(s) and not of MDPI and/or the editor(s). MDPI and/or the editor(s) disclaim responsibility for any injury to people or property resulting from any ideas, methods, instructions or products referred to in the content.